THE GEOLOGICAL SOCIETY OF AMERICA®

Rates and processes controlling periglacial alluvial fan formation: Implications for martian fans

Marisa C. Palucis[1,†], A.M. Morgan[2,3], J.V. Strauss[1], F. Rivera-Hernandez[1,4], J.A. Marshall[5], E. Menio[5], and R. Miller[1]
[1]*Department of Earth Sciences, Dartmouth College, 6105 Fairchild Hall, Hanover, New Hampshire 03755, USA*
[2]*Planetary Science Institute, 1700 East Fort Lowell, Suite 106, Tucson, Arizona 85719, USA*
[3]*Smithsonian Institution, Center for Earth and Planetary Studies, National Air and Space Museum, Washington, D.C. 20560, USA*
[4]*Earth and Atmospheric Sciences, Georgia Institute of Technology, 311 Ferst Drive, Atlanta, Georgia 30332, USA*
[5]*Department of Geosciences, University of Arkansas, 216 Gearhart Hall, Fayetteville, Arkansas 72701, USA*

ABSTRACT

Alluvial fans are found across a range of climates and are built from a combination of fluvial and debris flow processes. Correct identification of process is critical to reconstructing the climate and water histories of alluvial fans on Earth and Mars. Theory and data from subaerial Earth fans are often used to estimate paleoflow discharges and sediment fluxes for martian fans; however, most terrestrial work has been conducted on fans that are in hot, dry climates with runoff sourced from rainfall. This differs from the prevailing interpretation that martian fans were sourced from snowmelt under warming periglacial conditions. To characterize processes and rates of periglacial fan formation, we conducted a field-based study of the Black Mountain alluvial fan in the Aklavik Range, Canada. We observed active fluvial bedload transport as well as several small debris flows that had initiated from ice-filled gullies. Following a runoff event of ~0.005 mm/hr to ~0.2 mm/hr across the fan, we estimated sediment fluxes of ~0.04 m^3/hr. Under bankfull conditions, we estimated runoff rates between ~0.01 mm/hr to ~14 mm/hr and corresponding sediment fluxes of ~0.3 m^3/hr to ~550 m^3/hr. This suggests that moderate flow events, well below the maximum runoff production rates suggested for Mars, are capable of entraining and transporting appreciable amounts of sediment by fluvial processes. However, sedimentological and geomorphological observations suggest that ~67% of the fan was deposited fluvially; the remainder was deposited by mass flows. Our results emphasize the need to take care in interpreting martian sedimentary processes and climate from fan surface morphology alone.

INTRODUCTION

Alluvial fans are semi-conical sedimentary landforms that develop when channelized sediment and water exits a steep mountain front and emerges onto low-lying terrain, causing the channel to lose competence and capacity due to both a reduction in slope and lateral flow expansion (Blair and McPherson, 2009). Fans are built by a combination of fluvial and mass flow processes (Whipple and Dunne, 1992; Stock et al., 2008; Blair and McPherson, 2009; Stock, 2013). Fluvial flows have high water-to-sediment ratios, and fluid-particle interactions result in rolling, saltation, and dilute suspensions of sediment (Shields, 1936). Mass flows have low water-to-sediment ratios, and both solid and fluid forces influence downslope sediment motion (Iverson, 1997). Mapping of individual fan deposits, combined with relative and/or absolute dating techniques, have shown that both the mode and rate of sediment transport and deposition varies in time and space, and these factors have been linked to upslope changes in sediment supply and climate variations (see review in Stock, 2013).

Subaerial alluvial fans are found across a broad range of environments on Earth (referred to herein as "terrestrial fans") where there is sufficient topographic relief and high sediment production, including arid to semi-arid (e.g., Whipple and Dunne, 1992; Harvey, 1997; Blair, 1999b, 1999a, 2003), humid (e.g., Ori, 1982; Kochel and Johnson, 1984; Evans, 1991), alpine (e.g., Bardou and Delaloye, 2004; Crosta and Frattini, 2004; Cavalli and Marchi, 2008; Franke et al., 2015), and periglacial (e.g., Legget et al., 1966; Catto, 1993; de Haas et al., 2015b; Tomczyk and Ewertowski, 2017; Tomczyk et al., 2019) regions. They have also been discovered on Titan (Radebaugh et al., 2013; Birch et al., 2016), an icy moon of Saturn, and Mars (Moore and Howard, 2005; Morgan et al., 2018; Morgan and Wilson, 2019; Wilson et al., 2021). Alluvial fans on Mars have been of particular interest as crater statistics reveal that many were active during the Early Hesperian to Early Amazonian (ca. 3.4–1 Ga; Grant and Wilson, 2011; Mangold et al., 2012; Grant et al., 2014; Morgan et al., 2014; Holo et al., 2021), periods generally considered to be cold, dry, and unfavorable to significant fluvial activity (Carr and Head, 2010; Carr, 2012; Wordsworth, 2016). Detailed analyses of several individual martian alluvial fan systems, including estimates of fan volumes, flow discharges, and sediment concentrations, suggest that martian fans formed from hundreds to thousands of flow events over tens to hundreds of thousands of years and required significant water volumes (e.g., Morgan et al., 2014; Palucis et al., 2014; Kite et al., 2017), which is difficult to reconcile with the young age of these features. Within Gale crater, the Mars Science Laboratory *Curiosity* rover explored the distal end of the Peace Vallis alluvial fan and imaged fluvial clast-supported conglomerates with rounded pebbles (Williams et al., 2013). For these coarse-grained deposits to be transported, water depths of up to 0.9 m and flow velocities of up to 0.75 m/s would have been required (Williams et al., 2013; Dietrich et al., 2017). Some martian fans appear to exhibit a change in sedimentation process over time with a transition from fluvially dominated to debris flow-dominated processes (Williams et al., 2011), but it is unclear if this is due to changes in weathering rates, sediment yield, or the frequency and/or intensity of runoff-generating events.

Paleo-climate models of Mars during the Hesperian–Early Amazonian suggest that conditions may have been cold, icy, and snowmelt-dominated (Toon et al., 2010;

Marisa C. Palucis https://orcid.org/0000-0003-0034-5810
†marisa.c.palucis@dartmouth.edu.

GSA Bulletin;
published online 28 July 2022

https://doi.org/10.1130/B36459.1; 14 figures; 1 supplemental file.

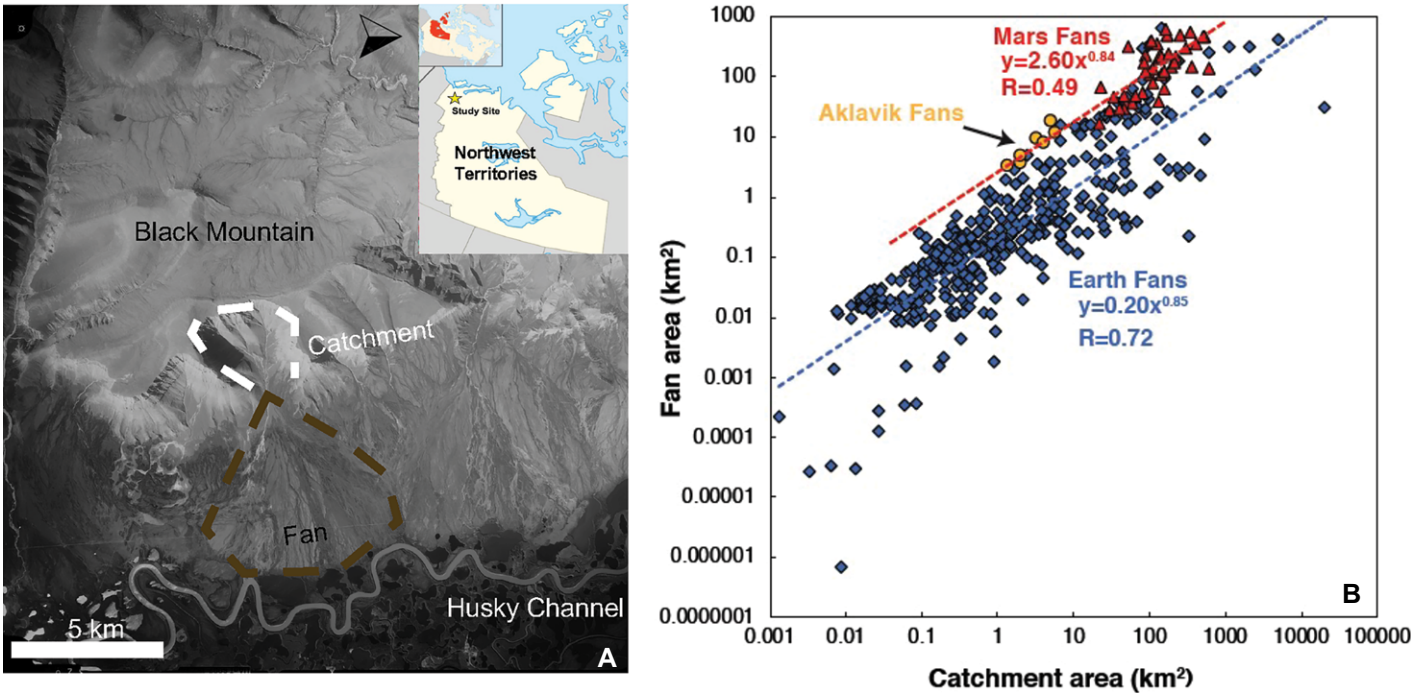

Figure 1. (A) National Air Photo Library (NAPL, Natural Resources Canada) image of the southern Aklavik Range shows the position of the Black Mountain fan relative to Black Mountain (Mount Goodenough) and the Husky Channel of the Mackenzie River, Northwest Territories, Canada. The catchment is outlined in white, and the fan deposit is outlined in brown. (B) Compilation of fan area versus catchment area for 433 terrestrial fans (blue); the Aklavik data are orange. Mars data (red) are from Moore and Howard (2005) and Kraal et al. (2008).

Wordsworth, 2016; Turbet et al., 2017; Weiss and Head, 2017), akin to periglacial environments on Earth, and possibly punctuated with periods of warming due to volcanic activity (e.g., Craddock and Greeley, 2009), impact events (Segura et al., 2008), methane release (Kite et al., 2017), or obliquity shifts (Laskar et al., 2004; Holo et al., 2018). However, almost all quantitative estimates of hydrologic conditions for fan formation are based on conceptual models and theory developed from Pleistocene–Holocene terrestrial fan systems in arid to semiarid and temperate climates (e.g., Blissenbach, 1954; Whipple and Dunne, 1992; Blair, 1999a; Harvey, 1999; Stock et al., 2008; Stock, 2013); thus, there is a lack of data and theory on the rates and processes controlling periglacial alluvial fan formation, and it is not clear whether current models (e.g., Stock et al., 2008) are applicable. The few previous studies that have been conducted on periglacial fans on Earth suggest that mass flow processes may dominate fluvial processes in building these deposits (Legget et al., 1966; Catto, 1993; de Haas et al., 2015a), but this has not been quantitatively assessed in terms of sediment transport rates or the actual volumes of sediment emplaced by fluvial, mass flow, or periglacial processes.

To determine how sediment production mechanisms and associated sediment transport rates and processes are reflected in alluvial fan morphology and sedimentology under a warming periglacial climate, we conducted field work on an alluvial fan underlain by continuous permafrost in the Northwest Territories (NWT) of Canada (Fig. 1A). Here, we (1) qualitatively describe the range of geomorphic processes occurring on this periglacial alluvial fan and its upslope watershed and compare them to prior observations and sedimentary deposits, (2) report flow discharges and runoff rates across the fan that occurred during an observed summer storm event, (3) estimate fluvial sediment fluxes using sediment transport theory for runoff rates comparable to those suggested for Mars, and (4) use field mapping and remote sensing analysis to determine the relative role and intermittency of fluvial versus debris flow processes in building a periglacial fan. Together, these data have important implications for water budget estimates and paleo-climate reconstructions on Mars as well as on Earth.

FIELD SETTING AND PREVIOUS WORK

Our study was conducted on the Black Mountain alluvial fan (67°55′09.37″N, 135°23′22.19″W) within the Aklavik Range, northeastern Richardson Mountains (Northwest Territories, Canada; Fig. 1A). Black Mountain is the Gwich'in name for what is referred to as Mount Goodenough on Canadian topographic maps. The fan emanates from a watershed along the eastern escarpment of the N–S-trending Aklavik Range (Fig. 1A). It was chosen due to its (1) position within a zone of continuous permafrost, (2) proximity to the local Arctic communities of Inuvik and Aklavik, (3) well-characterized geological setting, (4) prior geomorphic work conducted in the region in the 1960s–1980s (Legget et al., 1966; Catto, 1993), and (5) morphologic similarity to martian alluvial fans (Fig. 1B).

Tectonic and Geologic Setting

The Aklavik Range's eastern slope is a steep, locally fault-bounded escarpment that rises ~360–760 m above the western edge of the Mackenzie River floodplain. Uplift of the range is associated with Cordilleran orogenesis that likely initiated in the Paleocene–Eocene (65–50 Ma), with renewed regional exhumation in the late Eocene–early Oligocene (ca. 40–30 Ma) and the late Neogene (<8 Ma; O'Sullivan and Lane, 1997; Lane and Issler, 2011; McKay et al., 2021). Local to the field site, the Bug Creek fault (a strike-slip fault) has been mapped crossing the upper Black Mountain fan (Lane, 2005; Okulitch and Irwin, 2014; Fig. 2). The Richardson

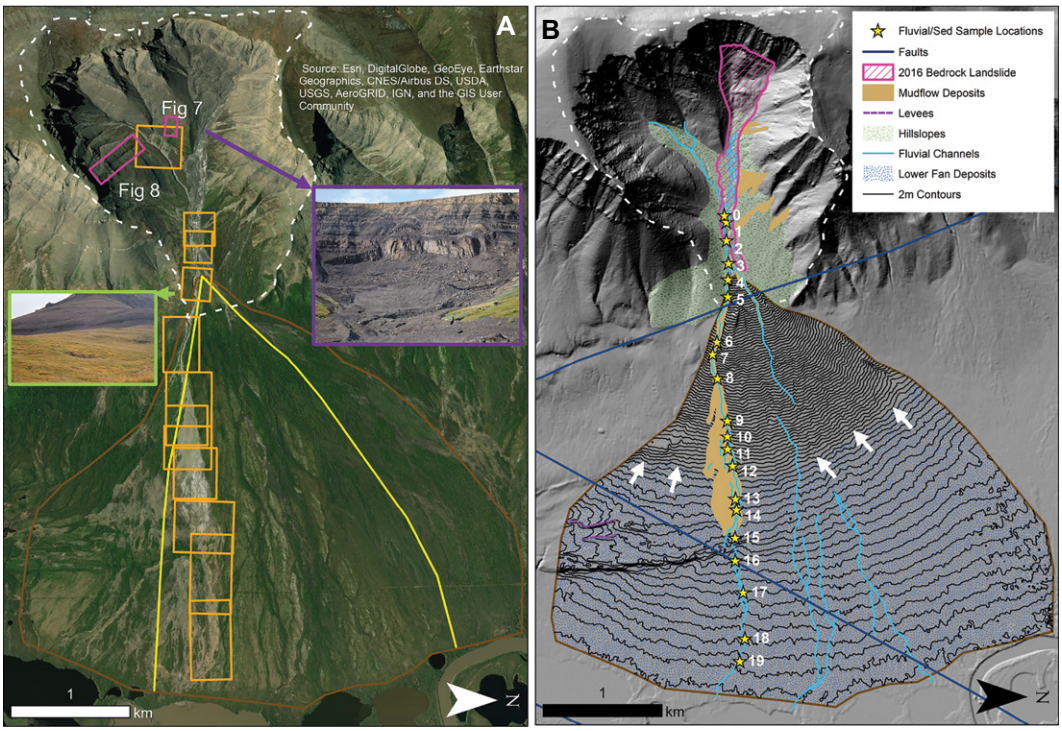

Figure 2. (A) Esri basemap of the site highlights the location of vegetation and recent mudflow activity as well as drone flight survey footprints (orange outlines). The elevation and slope longitudinal profiles in Figure 3 are shown in yellow. The inset outlined in green shows an example of the vegetated hillslopes connecting the catchment bedrock walls to the depositional fan, and the purple-outlined inset shows the steep catchment headwall, the 2016 landslide head, and the upper portion of the landslide deposit. (B) Modern-day geomorphic map of the Black Mountain fan overlies a hillshade image of the site derived from ArcticDEM data. White arrows point out the location of the slope break between the upper and lower portion of the fan.

Mountains are seismically active, with recorded M6–M7 earthquakes and frequent M3 tremors (Cassidy and Bent, 1993; Hyndman et al., 2005; Cassidy et al., 2005). Within the Aklavik Range, the seismicity is mainly driven by its localized strike-slip kinematics, with lateral deformation rates of ~2.1 mm/yr (Leonard et al., 2008).

The regional bedrock geology of the Aklavik Range consists predominantly of Upper Jurassic to Lower Cretaceous, siliciclastic-dominated marine strata (Dixon et al., 1992, 2019; Dixon, 1986; Dixon et al., 2008; Lane, 2005), as well as rare middle to late Paleozoic carbonate and siliciclastic rocks (Lane, 2005). The Black Mountain watershed drains sandstone- and shale-dominated strata of the Lower Cretaceous Martin Creek, McGuire, Kamik, Husky, Mount Goodenough, and Rat River Formations (Lane, 2005).

The Laurentide Ice Sheet reached its maximum extent on the eastern slopes of the Richardson Mountains at ca. 18 ka (Duk-Rodkin et al., 2004; Lacelle et al., 2013), but by ca. 13 ka, the Laurentide Ice Sheet most likely retreated completely from the Richardson Mountains region (Lacelle et al., 2013). Despite evidence for glaciation in the greater Richardson Mountains, the evidence is ambiguous in the foothills (Lacelle et al., 2013); most recent reconstructions suggest that the Aklavik Range remained unglaciated (Duk-Rodkin and Hughes, 1991; French, 2016; Lacelle et al., 2013). Regardless, the Black Mountain fan has likely been forming under a periglacial climate over the last ~13,000 yr (Legget et al., 1966).

Climate

The climate of the Aklavik Range is characterized by long winters with relatively little precipitation, mostly occurring as snow, with a Köppen climate classification of Dfc (continental subarctic climate). The summers (June–August) are generally short and mild, with frontal precipitation associated with maritime tropical cyclones (Bonsal and Kochtubajda, 2009). Climate data from Inuvik Airport show that annual rainfall is ~130 mm, most of which falls in July and August, and annual snowfall is ~136 mm (water equivalent; Hutchinson et al., 2009). Mean monthly temperatures are below freezing for six to eight months with only 50–90 frost-free days per year (Hutchinson et al., 2009). These data show that mean annual temperature has increased from ~–10.5 °C in the 1960s to ~–6 °C currently, with winter increases of up to 4 °C. Temperature amplitudes have decreased from ~36 °C in the 1960s to ~29 °C today.

Prior Geomorphic and Sedimentologic Observations

The Black Mountain fan and watershed were studied by Catto (1993) in the 1980s, and neighboring fan systems to the north (i.e., the Willow and Spruce alluvial fans) were studied by Legget et al. (1966) in the 1960s. Catto (1993) mapped a 3-m-deep main channel that extended down-fan to ~1.1 km from the Black Mountain fan apex, where it transitioned into mostly inactive, vegetation-covered, ~0.5-m-deep distributary channels. He observed active sediment transport within these ephemeral channels and noted that recent fluvial deposits were extensively modified by frost shattering, as well as occasional debris flow and mudflow activity. Regions between ephemeral stream channels had undulating topography, and occasionally there were subparallel ridges or stepped terracettes perpendicular to fan slope between 0.5 m and 1.5 m high. Catto (1993) interpreted these features to be the result of gelifluction or retrogressive thaw flow. He also observed spatulate projections of sediment 20–60 m long and 5–20 m wide on the southern margin of the fan, which were interpreted to be debris flow deposits. Interspersed between regions of debris flow and retrogressive thaw flow deposits were 0.3–1.5 m tundra polygons bordered by 5-cm-wide and 60-cm-deep ice wedges. At 18 locations on the upper fan, mid-fan, and fan toe zones, Catto (1993) described sedimentary successions exposed in cutbanks and hand-dug pits. On the upper fan, deposits were interpreted to be from debris flows triggered by snowmelt and slush avalanches. The sedimentary assemblages observed on the mid-fan were interpreted to be the result of both debris flow activity and low-velocity gelifluction. Along the fan toe, Catto (1993) interpreted the sedimentary assemblages to be the result of gelifluction. From his combined geomorphic and sedimentological

analysis, Catto (1993) concluded that the Black Mountain fan, as well as the other Aklavik Range fans, were formed predominately from debris flow and gelifluction events, which occur largely during spring snowmelt, with fluvial processes playing a minor role.

In contrast, observations by Legget et al. (1966) led them to suggest a fluvial fan formation mechanism for two fans ~15 km north of the Black Mountain fan, the Willow fan, and the Spruce fan. Their laboratory experiments showed that freeze-thaw processes could generate appreciable amounts of fine-grained sediment from sandstone and shale samples collected from the Willow fan watershed, and they inferred that these sediments could easily be transported during the summer from moderate, sustained snowmelt. Legget et al. (1966) observed a lack of fluvial incision ~1 km past the fan apex and irregular bedload deposition outside of defined channels, which they hypothesized to be the result of snowmelt debouching onto a frozen fan, leading to rapid spreading and thinning of streamflow and the deposition of sheets of sediment. To explain the abundance of silt within the boreholes that they drilled (~12 m deep), they suggested that post-depositional sediment breakdown must occur and must be associated with organic material inputs from sedge and grass growth during the summer months.

METHODS

This study builds on the work of Catto (1993) and Legget et al. (1966) and is based upon a combination of geomorphic and sedimentological fieldwork, high-resolution unmanned aerial vehicle (UAV)-derived topographic data, and sediment transport analysis. Field mapping and surveys (Fig. 2) were conducted over the course of three weeks in August 2019 following a summer storm event. Subsequent topographic and sediment transport analysis was performed using a combination of ArcticDEM data (2 m horizontal resolution with internal vertical accuracy of 0.2 m; Noh and Howat, 2015; Center et al., 2018) as well as new data provided by UAV-derived imagery.

Geomorphic and Sedimentologic Measurements

At 20 locations (stars in Fig. 2B) between the fan toe and ~0.5 km upstream of the fan apex (or head), defined as the location where the single-thread channel first bifurcates down-fan (Stock et al., 2008), we measured cross-sectional channel geometry, post-storm flow properties, and channel bed grain size distributions. These locations were predominately straight sections where bank formation was not controlled by vegetation or woody debris. At each location, we measured bankfull depth (H), active flow depth (h), bankfull width (W), active width (w), surface flow velocity (u_s), and bed grain size distribution, and identified bankfull geometry using criteria similar to that of Stock et al. (2008) (i.e., identifying the highest banks with recent activity, such as slackwater fines, matted vegetation, or gravel deposits, and avoiding cut banks, which might reflect historic incision). We measured surface flow velocity by noting the time taken for a float to travel over a 5 m downstream section of the channel. We measured the in-channel grain size distribution using a random walk technique similar to that of Stock et al. (2008). All grains were selected using the point of a mechanical pencil to prevent bias toward larger grains. The b-axes (intermediate axes) of at least 100 grains at all locations were measured to obtain statistically robust samples (Bunte and Abt, 2001). Within the active channel, we also noted the presence or absence of bedforms (e.g., step-pool, alternate bar, plane bed, etc.) and whether we observed active sediment transport of the coarse-grained load (i.e., bedload).

To determine whether ancient flow events were predominantly deposited as debris or fluvial flows (and to what extent they had been or were being modified by periglacial processes), we recorded sedimentological observations at 14 locations along the main incised distributary channel (Sites 2–15; Fig. 2B). At each station we documented grain size, sorting, and particle shape/fabric, as well as the absence or presence of sedimentary structures. We also noted sediment provenance, as well as occurrences of entrained vegetative debris and zones of bio- or cryoturbation.

Topographic Surveys and Derived Models

To capture high-resolution topography of the fan surface, we flew 16 UAV surveys using a DJI Phantom 4 Pro quadcopter. Each survey was flown at an altitude of ~50 m and covered an area ranging from 0.04 km^2 to 0.22 km^2 (mean 0.09 km^2), with a total coverage area of 1.09 km^2 (see extent in Fig. 2A; orange boxes). For each survey we generated 3-D point clouds using structure-from-motion in Agisoft Metashape and tied the 3-D model to ground control points collected with a Trimble R10 differential global navigation satellite systems receiver (DGNSS; horizontal accuracy of 0.6 cm and a vertical accuracy of 1 cm). Point clouds were then converted into ~2.5 cm/pixel resolution rectangular grid digital elevation models (DEMs). We converted the DEM raster into a slope map using the slope tool within ArcGIS Pro, which uses a 3×3 moving window of cells.

Process Domains and Sediment Budget

We identified process domains (i.e., steep uplands/sediment source region, colluvial, hillslopes, fluvial channels, and depositional fan) using a combination of imagery, topography, and field observations (Fig. 2). We used the World Imagery basemap in ArcGIS Pro for initial geomorphic mapping, which provides sub-meter imagery at our field site, and then ground-truthed (when possible) smaller-scale features such as fluvial channels. The Black Mountain watershed (white dashed outline in Figs. 1–2) is the upslope area that contributes sediment and water to the fan and was delineated using ArcticDEM topography (2 m/pixel) and the hydrology toolset (i.e., the Fill, Flow Direction, Flow Accumulation, and Watershed tools) within ArcGIS Pro. Flow direction was computed using the D-infinity algorithm (Tarboton, 1997). The hillslopes, which connect the steep bedrock walls to the alluvial fan, are mostly covered with tundra vegetation and were mapped based on a combination of visual and topographic data (green stippled region in Fig. 2B). The fan was mapped using topography (brown outline), where the fan is denoted by convex, 2 m interval contours, and recently active fluvial channels were mapped in regions of topographic convergence (i.e., concave-up in cross-section) and from imagery (aqua lines). We also mapped the extent of a landslide that occurred in 2016 (magenta hashed region) as well as recent (based on color and lack of vegetation) mudflow deposits and splays.

Fan volume was estimated in three different ways. The first used the geometric model of Giles (2010). The second assumed that the fan was at least as deep as the Willow fan to the north (~12 m deep; Legget et al., 1966), so we simply multiplied that depth by the fan area. The third method used the surrounding topography to reconstruct the contours underneath the fan to estimate the pre-fan surface (Palucis et al., 2014). The reconstructed pre-fan surface was then subtracted from the modern-day topography to determine the fan volume. We obtained the total sediment volume within the fan by taking the fan/deposit volume and multiplying it by $(1–\lambda)$, where $\lambda = 0.35$ is the porosity (using the average porosity of silty soil; Selby, 1993). To estimate the volume of sediment eroded from the 2016 landslide, we projected a smooth surface between the bounding sidewalls of the landslide scar. This projected surface was then converted into a gridded DEM and subtracted from the current-day topography.

Fluvial Runoff and Sediment Transport Model Formulation

A key goal of this work was to estimate fluvial discharge and runoff rates on a periglacial fan, which we can compare to modeled rates for Mars, and to calculate fluvial sediment fluxes using sediment transport theory. We first calculated post-storm discharge (Q) and bankfull discharge (Q_{bf}) at each channel cross-section location using principles of continuity:

$$Q = a_{xs}u \quad (1)$$

$$Q_{bf} = A_{xs}U \quad (2)$$

where the mean post-storm velocity (u) in the channel was estimated to be $2/3u_s$, assuming a log linear velocity profile (Garcia, 2008), and a_{xs} and A_{xs} are the post-storm and bankfull cross-sectional channel areas calculated using topographic cross-sections from the UAV-derived DEM and the water stage (i.e., h or H). The bankfull velocity (U) was calculated using the Darcy-Weisbach equation:

$$U = \sqrt{\frac{8gHS}{f}} \quad (3)$$

where S is the fluid surface slope, g is gravity (9.8 m/s^2), and f is the Darcy-Weisbach friction factor, a quantification of flow resistance. We assumed uniform flow such that the fluid surface slope equals the local bed slope. Local bed slope was measured using our UAV-derived DEMs from long profiles that extended 5 m upstream and 5 m downstream of each cross-section. Ferguson (2007) derived an empirical expression for f that is intended to work for a range of flow conditions and a range of channel slopes:

$$\sqrt{\frac{8}{f}} = 17.7\frac{h}{D_{84}}\frac{1}{\sqrt{52.3 + 5.57\left(\frac{h}{D_{84}}\right)^{5/3}}} \quad (4).$$

Runoff (i.e., m/s) at each cross-section was calculated by taking discharge (Q) and dividing by the upslope contributing drainage area (A_d), which was calculated using the ArcGIS hydrology tools.

To understand the significance of the observed flow event in building the fan, we estimated when the non-dimensional boundary shear stress on the bed and banks (τ^*) is above a representative critical boundary shear stress for the initiation of motion (τ^*_{cr}) (Parker, 1978; Ikeda et al., 1988; Parker et al., 2007; Seizilles et al., 2013), which often occurs as flows approach bankfull discharge in temperate alluvial systems (e.g., Parker, 2008). The non-dimensional bed shear stress, or Shields stress, is defined as:

$$\tau^* = \frac{\tau_b}{(\rho_s - \rho)gD_{50}} = \frac{\rho g R_h S}{(\rho_s - \rho)gD_{50}} \quad (5)$$

where τ_b is the dimensional bed shear stress, R_h is the ratio of the flow area to its wetted perimeter within a channel, ρ is the fluid density, ρ_s is the sediment particle density, and D_{50} is the median grain size of the bed surface. Unless specified otherwise, the critical boundary shear stress, τ_{*cr}, is calculated using the slope-dependent relation from Lamb et al. (2008):

$$\tau^*_{cr} = 0.15S^{0.25} \quad (6).$$

The Lamb et al. (2008) relationship was empirically derived using systems with gravel or coarser sediment. As many of the sites along the fan contained a significant proportion of material $\leq$2 mm, we used the Wilcock and Crowe (2003) model, which accounts for mixed sand-gravel systems, to estimate τ^*/τ^*_{cr} and total non-dimensional sediment fluxes (W^*_{tot}) during the storm event and under bankfull conditions:

$$W^*_{tot} = \begin{cases} 0.002(\tau^*/\tau^*_{rm})^{7.5} \; for \; \tau^*/\tau^*_{rm} < 1.35 \\ 14\left(1 - \frac{0.894}{(\tau^*/\tau^*_{rm})^{0.5}}\right)^{4.5} \; for \; \tau^*/\tau^*_{rm} \geq 1.35 \end{cases} \quad (7a, 7b)$$

where

$$\tau^*_{rm} = 0.021 + 0.015exp\left[-20F_S\right] \quad (8)$$

and F_s is the percent sand on the bed surface. Volumetric particle bedload transport rates ($q_{b,vol}$) per unit width (m^3 s^{-1} m^{-1}), for grain sizes within the range of bed material (i.e., larger than silt), were then calculated using

$$q_{bVol} = \frac{W^*_{tot}u^3_*}{\Re g} \quad (9)$$

where $u^* = \sqrt{\tau_b/\rho}$ is the shear velocity and $\mathcal{R}$ is the submerged density of quartz (1.65).

Bedforms and other sources of macro-scale roughness affect flow resistance and thus impact values derived using Equations 5–8. We account for this by estimating τ^*/τ_c^* and coarser grained (>4 mm) bedload fluxes using the empirical model of Schneider et al. (2015). This sediment transport model, developed using field data from sites that cover a wide range of channel slopes, flow discharge rates, and grain sizes, is a modified form of the Wilcock and Crowe (2003) formulation. The total non-dimensional transport rate (W^*_{tot}) is a function of both the median grain size (D_{50}) of the coarse grain size distribution and the ratio of the total dimensionless boundary shear stress on the bed (τ^*) to the reference shear stress (τ_r^*), where the reference shear stress τ_r^* is defined as

$$\tau_r^* = 0.56S^{0.5} \quad (10).$$

The non-dimensional bedload transport model is:

$$W^*_{tot} = \begin{cases} 0.002(\tau^*/\tau^*_r)^{16.1} \\ \quad for \; \tau^*/\tau^*_r < 1.2 \; and \; D_{50} > 4mm \\ 14\left(1 - \frac{0.85}{(\tau^*/\tau^*_r)^{0.7}}\right)^{4.5} \\ \quad for \; \tau^*/\tau^*_r \geq 1.2 \; and \; D_{50} > 4mm \end{cases} \quad (11a, 11b).$$

Volumetric bankfull bedload transport rates ($q_{bf,vol}$) per unit width (m^3 s^{-1} m^{-1}) were then calculated using Equation 9.

Intermittency (I_f) is the fraction of time over which bankfull conditions would complete an equivalent amount of sediment transport as the river's normal hydrograph (Paola et al., 1992; Hayden et al., 2021). To estimate the duration of fluvial activity on the Black Mountain fan, we estimated I_f as:

$$I_f = \left(\frac{V_{fan,fluv}}{Age_{fan}}\right)/\left(Wq_{bf,Vol}\right) \quad (12)$$

where $V_{fan,fluv}$ is the volume of the deposit assumed to be fluvial in origin (based on our field and remote sensing mapping), the product $Wq_{bf,Vol}$ is the volumetric bankfull bedload transport rate (m^3 s^{-1}), and the inferred age of the fan (Age_{fan}) is the time since the retreat of the Laurentide Ice Sheet from the region (~13,000 yr; Lacelle et al., 2013). This analysis assumes that (1) the Black Mountain fan captures all bedload material (i.e., all grains >2 mm), though we recognize it is likely not a perfect sink; (2) the current fan deposit is entirely post-Last Glacial Maximum (Legget et al., 1966; Catto, 1993); and (3) based on the short timescales, accommodation space due to faulting has not changed appreciably. As fans can have multiple channel threads active during a bedload transporting event, the intermittency factor includes a degree of inherent uncertainty surrounding the unknown number of active channels at any given time.

OBSERVATIONS AND INTERPRETATIONS

Geomorphology of the Black Mountain Fan

Based on topography, we mapped the modern-day extent of the Black Mountain fan to be ~9 km^2, which is fed by a ~4 km^2 catchment. The catchment has an average relief of ~450 m and a drainage density of 0.09 km^{-1}. In comparison, the fan volume is estimated to range from 0.043 km^3 (empirical model from Giles, 2010) to 0.11 km^3 (fan area × depth), with an intermediate estimate of 0.049 km^3 (topographic reconstruction of the pre-fan surface). Longitudinal elevation profiles from the fan apex to its northern and southern distal ends are concave-up (typical of fluvial-dominated alluvial fans; Stock et al., 2008), though the upper portion of the fan (unshaded region, Figs. 2B and 3) is linear to slightly concave-up (similar to debris flow–dominated fans in California, USA (Whipple and Dunne, 1992), and Svalbard, Norway (de Haas et al., 2015b). The upper ~2 km^2 area of the fan is topographically steeper, with average slopes of 0.084 ± 0.036. Slopes of the lower fan average 0.031 ± 0.025. The longitudinal and slope profile down the southern margin of the fan shows a ~2 m scarp on the lower fan, with local slopes approaching 0.45. The origin of this geomorphic feature is likely a large slope failure that occurred out of the catchment to the south (Catto, 1993), but it could also be a fault scarp.

The primary distributary channel is up to 10 m deep near the fan apex. In contrast, Catto (1993) reported depths of only up to 3 m, which indicates 7 m of incision over the last ~30 yr. Older, abandoned channels are marked by dense vegetation and low albedo and only occasionally show evidence of recent flood or mudflow inundation (based on field examination and the World Imagery basemap in ArcGIS Pro). Bankfull channel widths on the main channel range between ~1 m and 10 m; there is no clear trend with width downstream, but width does show a slight positive correlation with local channel slope (Fig. 4A). Bankfull channel depths range between ~0.05 m and 0.5 m, and like bankfull width, there is no clear trend with depth downstream, but there is a slight positive correlation between bankfull depth and slope (Fig. 4B). Width-to-depth ratios for most of the channels on the fan fall between ~10 and 100 (Fig. 4C).

Median grain sizes within the channels fine down-fan (using the full distribution; i.e., including the ≤2 mm grains), going from coarse gravels at the apex, to fine to medium gravels mid-fan, and coarse sand at the distal end (Supplemental Material Table S1[1]), but the median size of the gravel fraction did not change appreciably for the upper ~70% of the fan (Fig. 5A). The percentage of fine-grained material (≤2 mm fraction) was observed to increase linearly down-fan from ~10% to 50% (Fig. 5B). Observed channel morphologies range from cascade near the fan apex (~0.06 ≥ S ≥ ~0.12) to plane bed (~0.02 ≥ S ≥ ~0.12) to step-pool (~0.07 ≥ S ≥ ~0.08) to alternate bar (~0.01 ≥ S ≥ ~0.1; Fig. 6). Most of the channels we mapped on the fan were alternate bar in form (14 of the 19 sites; Table S1), where the bars ranged from coarse gravel bars on the upper fan to silty-sand bars on the lower fan. A majority of the fluvial channels on the fan are steep alluvial streams (S > ~0.02) (Montgomery and Buffington, 1997). The bedforms in these channels appeared to be the result of both fluvially transported sediment (based on clast-supported deposits and imbrication of the coarse- and fine-grained gravels) and reworked coarse-grained debris flow or landslide deposits (e.g., coarser grains that formed step-pool–like morphologies in the channels but lacked imbrication and showed winnowing of the finer-grained matrix).

We mapped several recent mass flow events, both within the catchment and on the fan. Most notable was a 2016 (based on review of Landsat imagery) landslide deposit that initiated from the east-facing bedrock wall of the catchment and delivered ~1.5*10^5 m^3 of sediment to the upper fan (black hatching in Fig. 2). Smaller landslides occurred during our 2019 field expedition. In one event, the initiation zone was ~2 m wide, and the failure plane appeared to be along exposed ice (Fig. 7A). Failure initially incised a ~1-m-wide channel just downslope from the initiation zone (Fig. 7B), followed by a granular

[1]Supplemental Material. Table S1: Channel parameters and sediment flux during August 17th 2019 storm conditions. Table S2: Channel parameters and sediment flux under bankfull conditions. Please visit https://doi.org/10.1130/GSAB.S.20075870 to access the supplemental material, and contact editing@geosociety.org with any questions.

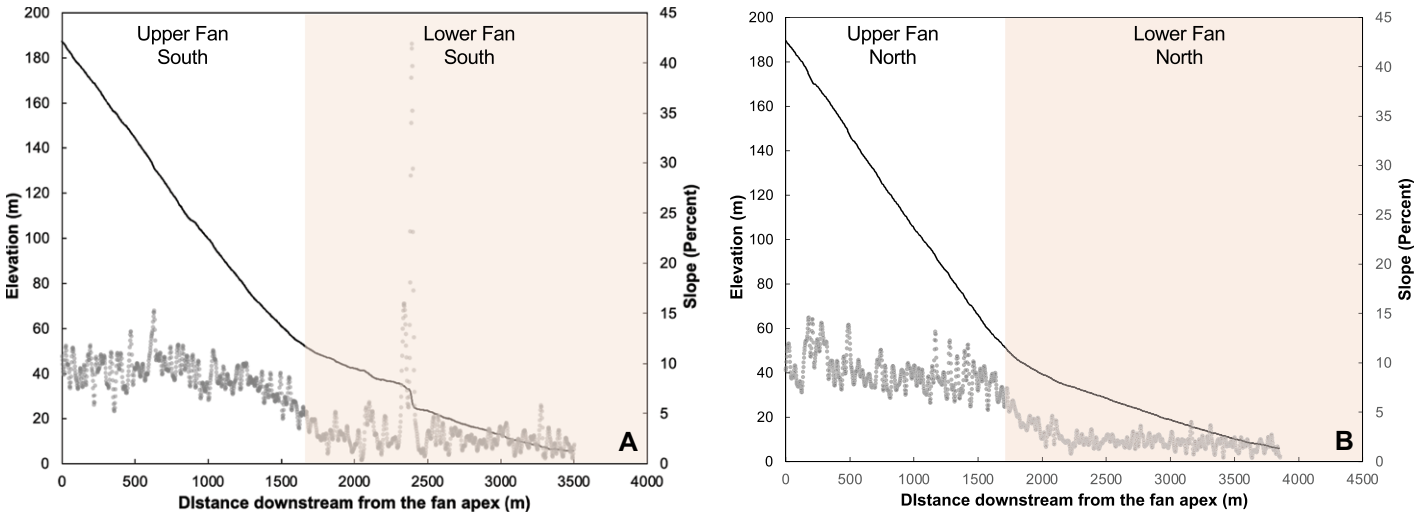

Figure 3. (A) Fan longitudinal elevation profile (black line, left axis) and slope (gray dots, right axis) down the southern margin of the fan were developed using ArcticDEM topographic data. (B) Fan longitudinal elevation profile (black line, left axis) and slope (gray dots, right axis) down the northern margin of the fan were developed using ArcticDEM topographic data. Profiles were taken perpendicular to contour (Fig. 2A), and for the southern margin they follow the active river channel. Slopes (percent) were calculated using the Slope tool within ArcGIS Pro.

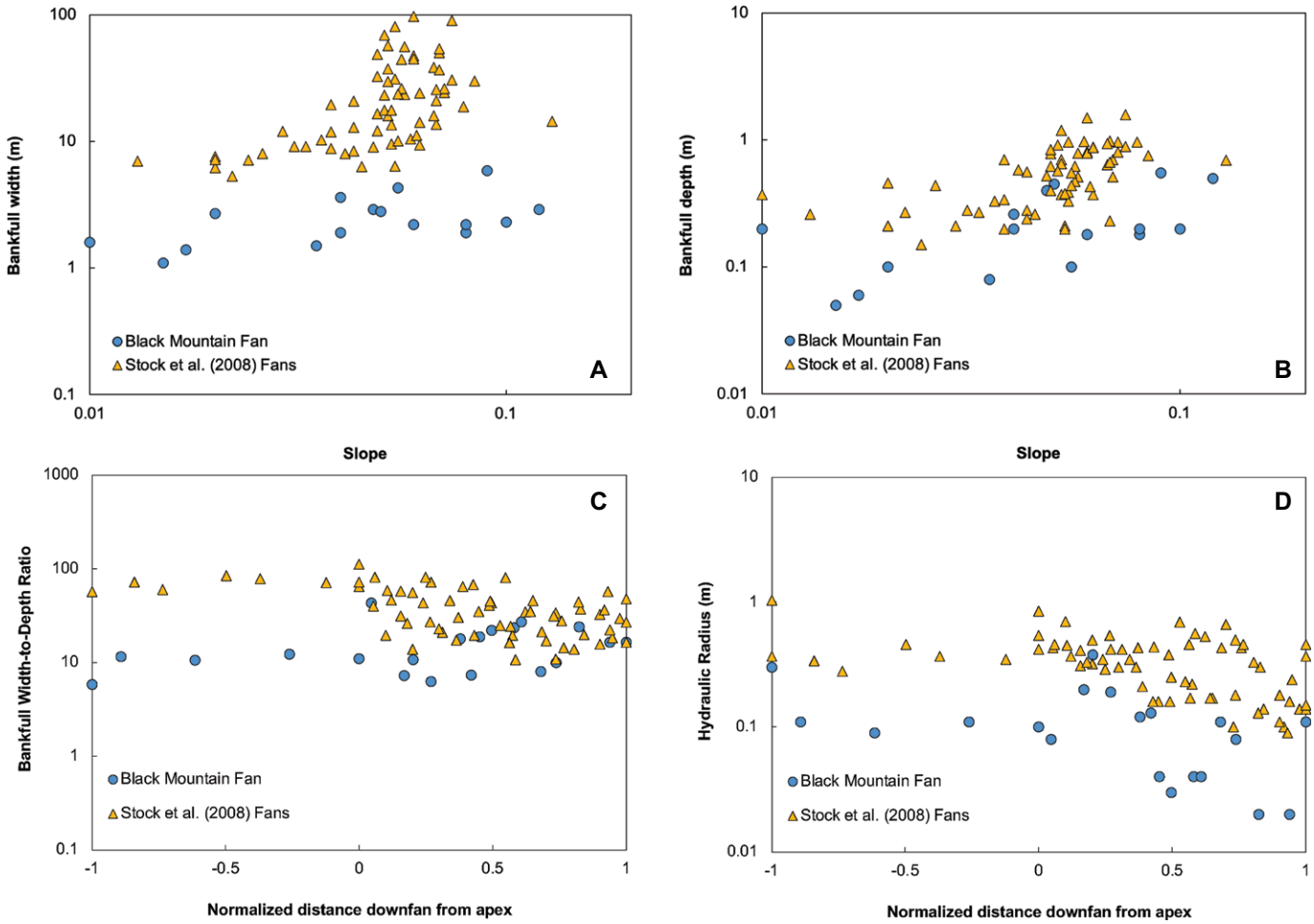

Figure 4. Bankfull (A) channel width and (B) depth show a slight increase with channel slope for both the Black Mountain fan (blue dots) and the Mojave fans investigated by Stock et al. (2008) (orange triangles). (C) Width-to-depth ratios for both the Mojave fans and the Black Mountain fan range between ~10 and 100, and there is no clear trend with distance downslope. (D) The hydraulic radius for both the Mojave fans and the Black Mountain declines slightly down-fan from the fan apex (where the fan apex is at 0 on the *x*-axis; negative values are upstream of the apex, and positive values are downstream of the apex).

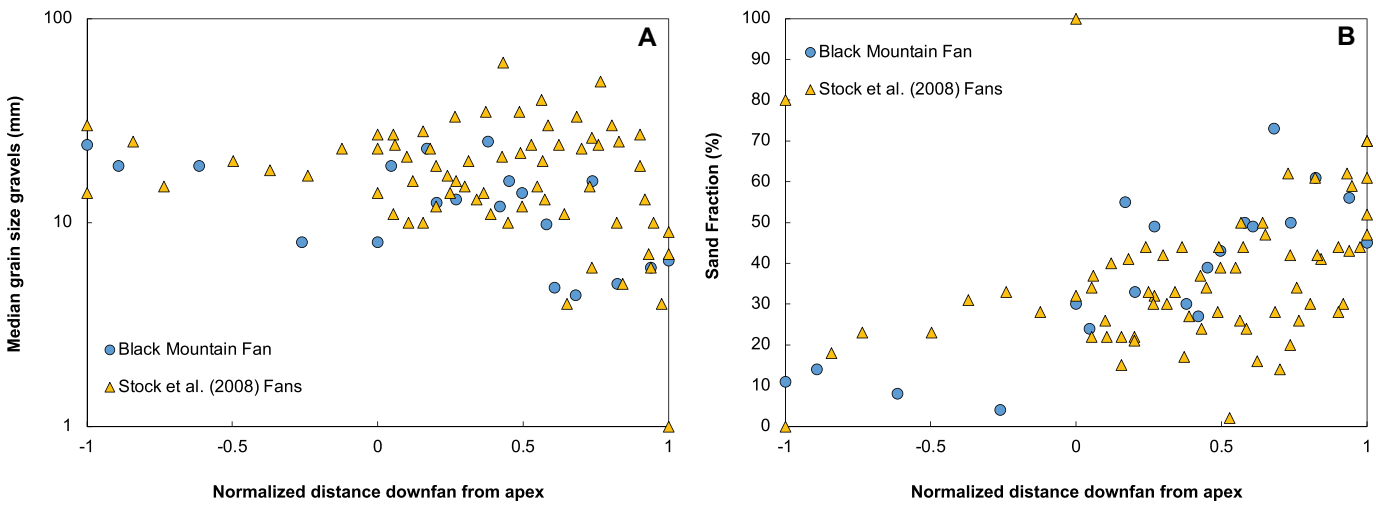

Figure 5. (A) Median grain size of the gravel fraction remains relatively constant down-fan from fan apex (at 0) for the upper ~60%–70% of the fan channel lengths for both the Black Mountain fan and those studied by Stock et al. (2008). (B) Plot shows increasing bed area sand fraction with distance from the fan head (at 0).

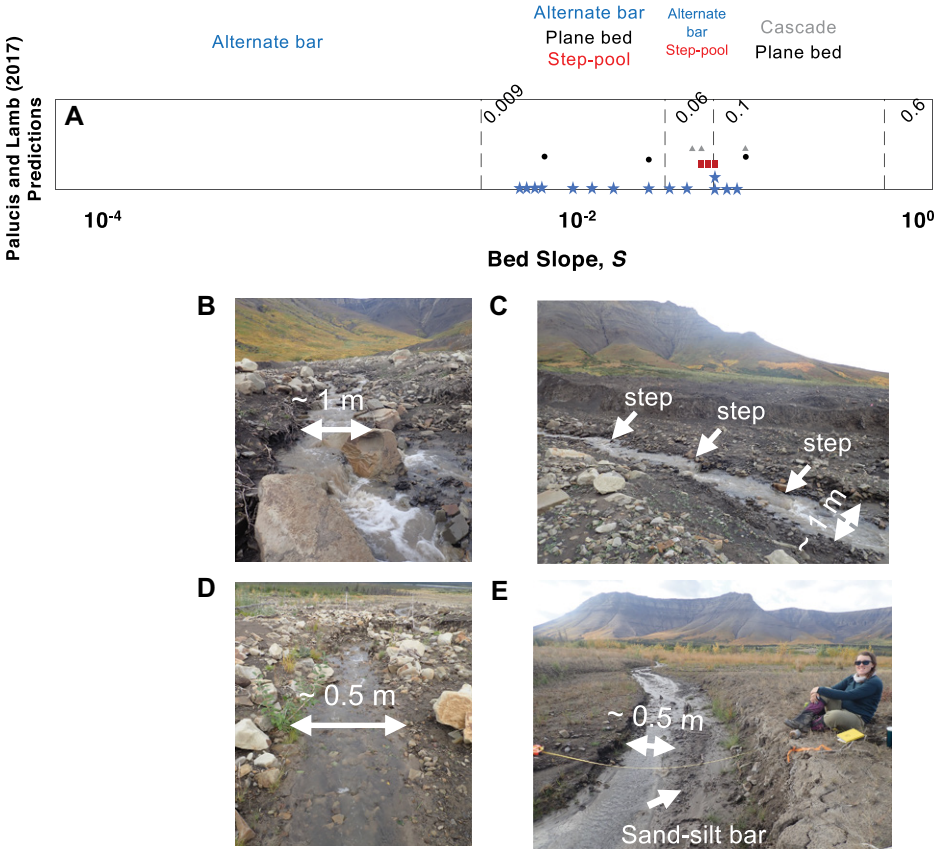

Figure 6. (A) Predictions for channel slopes are shown where alternate bar (blue stars), plane bed (black circles), step-pool (red squares), and cascade stream (gray triangles) morphologies would be found using theory for alluvial streams (Palucis and Lamb, 2017). Our observations for different stream morphologies on the Black Mountain fan fit these predictions well, except for cascade streams, which were mapped at lower-than-expected channel slopes. (B) Cascade stream morphology. (C) Step-pool stream morphology with white arrows pointing out the steps. (D) Plane bed morphology. (E) Alternate bar morphology.

debris flow that flowed ~100 m downslope, as evidenced by coarser-grained levees spaced ~0.2 m apart (Fig. 7C). The failure mechanism appeared to be repeated saturation and fluidization of the fine-grained shale talus. We also observed several small debris flow deposits that appeared to have recently initiated from an ice-filled gully. The flows ran out ~65 m and terminated in lobate snouts containing up to ~20 cm clasts (Fig. 8A). At least two flow events occurred based on cross-cutting relationships between sets of paired levees (Fig. 8B). Several recent mudflow events were also observed to have initiated within the catchment's south-facing walls and onto the fan (using aerial imagery), the largest of which was transported through the fan's southern channel, resulting in overbank deposition of mud along the upper channel and a large mud splay mid-fan (tan regions in Fig. 2B). Older, lower albedo mudflow deposits are also visible in Landsat and Worldview-3 imagery, most of which are concentrated on the southern half of the fan (Fig. 2). We did not observe the ~20–60-m-long, ~5–20-m-wide lobate deposits (debris flow deposits) described by Catto (1993) along the southernmost fan margin. We did, however, observe what appeared to be a paired levee deposit above the 2-m-high topographic step mid-fan on its southern edge (purple dashed lines in Fig. 2B).

Catto (1993) noted that periglacial features, including polygonal cracks and frost mounds, were pervasive across the fan surface. We found these to be muted and restricted to the uppermost, steeper sections of the fan. Due to the thick vegetation present during our field season, we also did not observe any sub-parallel ridges

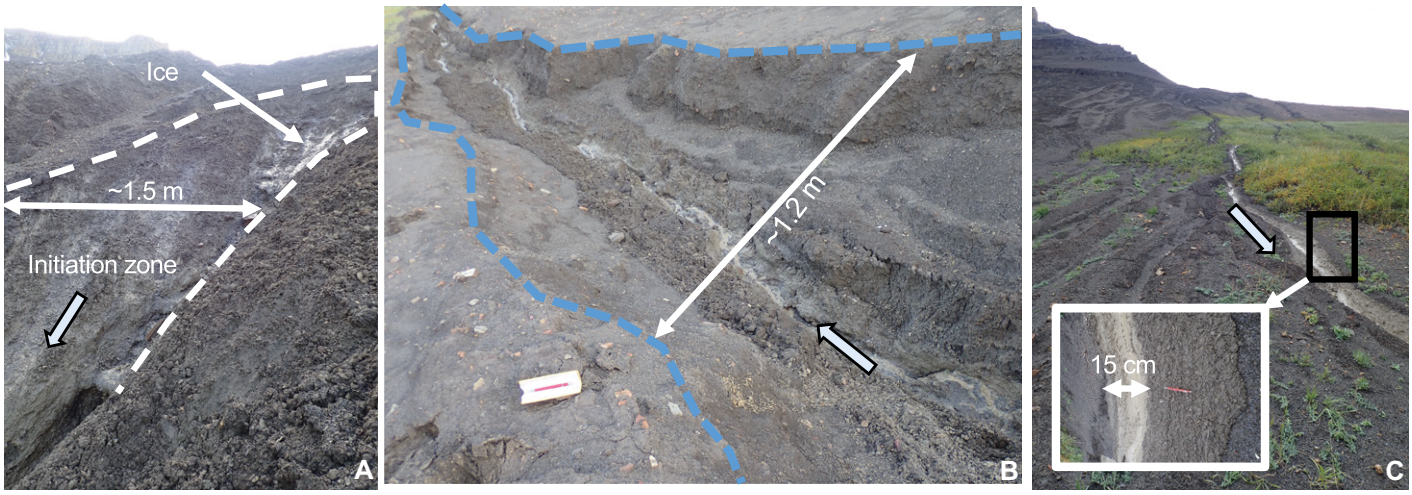

Figure 7. Examples of deposits resulting from small landslides during the 2019 field campaign are shown. (A) Initiation zone of a shallow landslide occurring in fine-grained shale talus, where massive ice is observed ~1 m deep. (B) Main channel that was incised into the talus ~10 m downslope of the failure head scarp, as well as at least two subsequent flow events. (C) Channel ~100 m downslope of the failure head scarp where coarse-grained overbank deposition was observed.

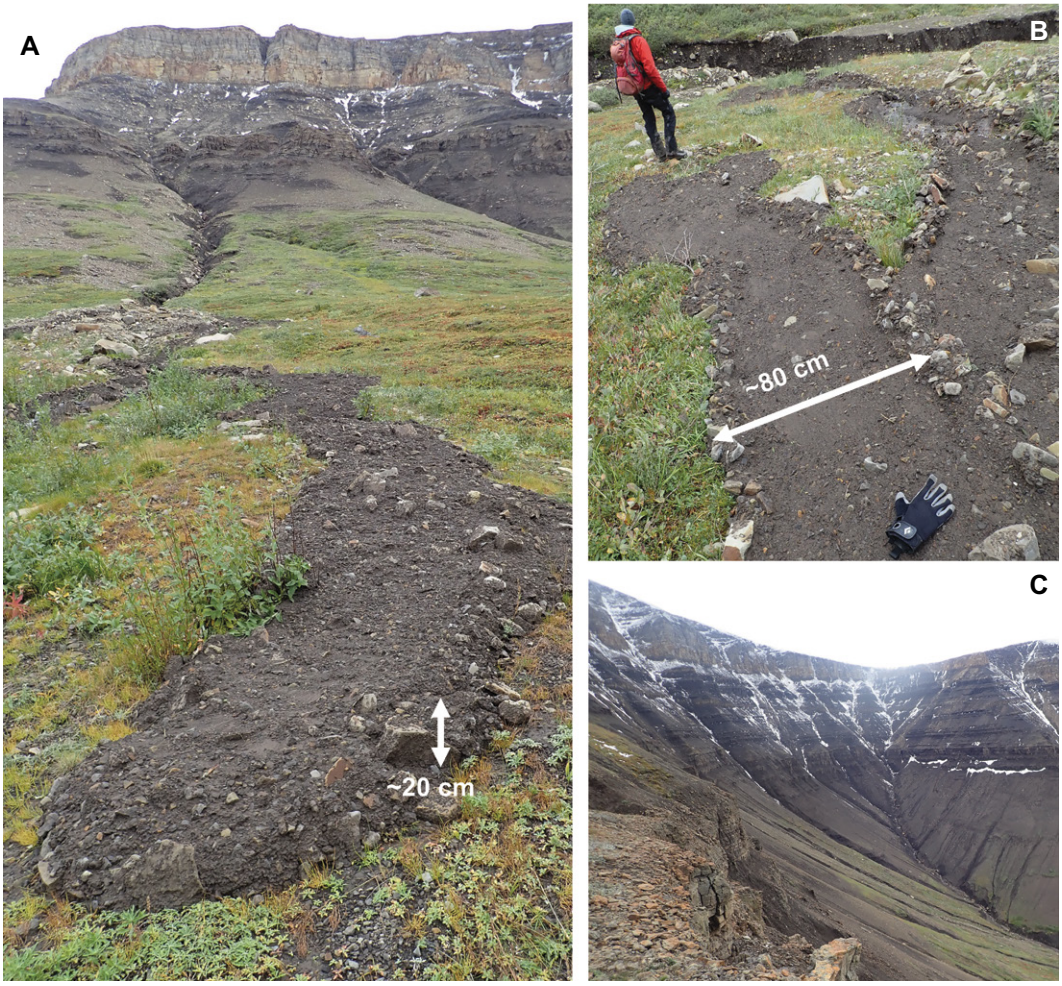

Figure 8. (A) Photo shows a recent debris flow event that initiated from snowmelt and runoff from steep gullies incised into the sandstone cliffs above; clasts as large as ~20 cm were observed in the flow front (the lobate snout). (B) Debris flow channels, bounded by coarse-grained, self-formed levees, were ~80 cm to 1 m wide. (C) Image of the Black Mountain catchment immediately after the snowfall event shows where snow and ice accumulated.

and stepped terracettes on the mid-fan that Catto (1993) inferred were from progressive gelifluction of the fan surface, nor could we identify these features in the topographic data (ArcticDEM or UAV). We did observe many shale boulders and clasts that were affected by frost weathering and shattering on the upper and mid fan, both in the fluvial channels and on the fan surface (Fig. 9). The resulting shale chips tended to be subangular and were ~2–4 mm in size (i.e., fine-gravel). The hillslopes surrounding the fan, which were largely covered by tundra vegetation (green stippling in Fig. 2), did show evidence of small solifluction lobes and hummocks. On steeper portions of the hillslopes, we observed active layer detachments and a few small detachment scars.

Sedimentology of the Black Mountain Fan

On the upper fan (sites 0–12), we documented ~0.75-m-thick to ~10-m-thick exposures of ancient fan deposits composed of two dominant sedimentary facies (Fig. 10). Facies A (Figs. 10A–10B) consists of matrix-supported pebble to boulder conglomerate with medium-sized pebbles to large cobbles with occasional boulders. The clasts are predominantly composed of sandstone with rare granitoid and carbonate lithologies, and they are commonly angular to subrounded, poorly to very poorly sorted, lack imbrication, and are supported by a silt- to mud-sized matrix. These deposits are massive, lack grading, and range from ~40%–60% matrix (by volume). The bedding thicknesses range from ~50–900 cm but are typically ~100–150 cm. The bedding bounding surfaces tend to be planar and are mainly differentiated by changes in the proportion of matrix to coarse-grained clasts.

Facies B (Fig. 10C) consists of coarser-grained, clast-supported conglomerate with clasts ranging from pebble to boulder size, though the proportion of larger clasts increases near the fan apex. The clasts are similar in composition to Facies A and are subangular to subrounded, poorly to very poorly sorted, and have subtle imbrication. Clasts tend to be tightly packed in clast-supported beds with ~5–10% of the bed comprising a silt- to sand-sized matrix. No internal sedimentary structures or grading are apparent within this facies. Individual beds of Facies B range from ~25 cm to 100 cm thick, but they are typically ~50 cm thick.

We found that Facies A represented ~71% of the exposures at the observed stations on the upper fan, while Facies B represented ~18%, and soil (i.e., material affected by vegetation) represented the remaining ~11%. There was no clear trend in facies type with distance downstream. Interstitial ice and ice lens were not observed within any of the deposits, but there was often a ~50–100-cm-thick soil horizon at the top of each section with evidence of cryoturbation and mechanical breakdown of shale into small fragments due to freezing and thawing.

Facies A is typical of a debris flow deposit and is likely the diamicton strata described by Catto (1993) on the upper fan. He suggested that rapid snowmelt within the catchment and/or permafrost melt within the hillslope soils or talus can trigger debris flows, and the large proportion of fine-grained material aids in the propagation of the flow downslope due to elevated pore pressures. This scenario is similar

Figure 9. (A) A frost-shattered boulder within the recent 2016 landslide deposit is shown; (B) a frost-shattered shale clast shows a rapid breakdown of shale grains relative to the sandstone grains.

to the smaller-scale flow event we observed in the field (Fig. 8), so it is possible that Facies A reflects recent deposits of similar origin. In contrast, Facies B is predominately clast-supported and is instead interpreted to be the result of fluvial sediment transport and deposition, likely by high-energy water flows. The thickness of these deposits is similar to the thickness of the sediment beds within the modern-day fluvial channels, the range of observed grain sizes is similar between the modern channels and these deposits, and there is a general decrease in median grain size with distance downslope, which is typical of fluvial systems.

On the lower fan, exposures of ancient fan deposits were ~1 m thick and consisted of a single facies: Facies C (Fig. 10D). These deposits are composed of cohesive silty clay layers that are ~5 cm thick and alternate with layers of structureless, orange-colored silt (~5–10 cm thick). The silt layers occasionally contain imbricated fine- to medium-grained pebbles. Organic detritus and roots are present along some contacts between the silt and clay layers, and interstitial ice was observed after digging ~0.5 m into a channel wall. The lower fan deposits are commonly overlain by ~0.5–0.75 m of soil/tundra.

Similar sedimentological observations of our Facies C were made by Catto (1993), who interpreted these alternating layers to be the result of slow-moving gelifluction deposits from previously deposited debris flows (i.e., silty clay layer) with occasional sheet flow or non-channelized fluvial flow (i.e., silt layer). Based on modern-day surface processes occurring on the lower fan, we instead interpret these layers as being predominantly fluvial in origin, where the silt-gravel layers are recording past channel threads and the silt-clay layers are recording either overbank deposition during larger flood events, sheet

Figure 10. Photographs show typical sedimentary units exposed along the incised channels going down-fan; (A) and (B) are examples of Facies A, matrix-supported coarse gravel and boulders, which are inferred to be debris flow deposits. (C) An example of Facies B, clast-supported pebbles and gravels overlain by a sand-silt lens, which is inferred to be a fluvial deposit. (D) An example of Facies C, a silt- and clay-rich (likely) flood deposit.

flows, or hyper-concentrated or mudflow events that splay out of the channel. The presence of ice within the deposits could imply that gelifluction or solifluction is occurring post-deposition, though we did not observe obvious evidence of these processes occurring at the surface.

Field Observations from Summer 2019 Storm Event

A summer storm event occurred during our field campaign on 17 August 2019. Snow and ice was limited to the fan catchment and was concentrated within bedrock gullies, while rain occurred across the lower fan. As such, runoff to the upper fan and fan apex was likely dominated by snowmelt while the lower fan experienced a mix of rainfall and snowmelt. From a rain gauge deployed near the fan toe, we estimate maximum rainfall rates of up to 5 mm/hr (measured over 30 min) with average rainfall rates of 2 mm/hr. Immediately post-storm, we recorded flow properties of the activated main channel: flow depths ranged from 0.025 m to 0.13 m, flow widths from 0.05 m to 0.72 m, and flow velocities from 0.4 m/s to 1.3 m/s. Gravel bedload transport was observed at three locations on the channel, Sites 1 and 2, which are located just above the fan apex, and Site 14, located on the large, recent mud splay. We did not have sediment traps to measure actual bedload fluxes, but gravel-sized grains were observed saltating along the bed and across our cross-section tapes every few seconds.

ANALYSIS

Modern-Day Flow and Sediment Transport Rates

We estimated water discharge and runoff for both the 2019 storm event as well as for bankfull flow conditions using Equations 1–4 (Tables S1 and S2; see footnote 1). During the August 2019 event, discharge decreased from ~0.1 m^3/s at the uppermost sites down to ~0.01 m^3/s at the fan's distal end, which correspond to runoff rates of ~0.1–0.2 mm/hr to ~0.01 mm/hr, respectively. This was likely due to a combination of infiltration, evaporation, and distributary channels dividing water (e.g., Stock, 2013). Under bankfull conditions, we estimate that discharges on the upper fan may be as high as ~6–12 m^3/s and decrease down to ~0.02–0.4 m^3/s at the fan's distal end, which correspond to runoff rates of ~7–14 mm/hr down to ~0.01–0.02 mm/hr. Non-dimensional bed shear stresses under storm conditions were estimated using Equation 5 (Fig. 11A), and the critical Shields stress (τ^*_{cr}), the threshold at which sediment starts to move, was estimated using Equations 6 and 8. Bankfull sediment transport theoretically occurs when the ratio of the Shields stress to the critical Shields stress is greater than 1. When using the Lamb et al. (2008) criterion, we found that moderate to intense bedload is predicted to occur at all sites ($1.2 < \tau^*/\tau^*_{cr} < 9.1$) but Sites 9 and 19, and using the Wilcock and Crowe criterion, intense bedload is predicted at all locations ($1.9 < \tau^*/\tau^*_{cr} < 28$; Table S1). This differs from our actual observations of low to moderate bedload transport occurring only at Sites 1, 2, and 14. Critical non-dimensional bed shear stresses were also estimated using the Schneider et al. (2015) model (Equation 10), which attempts to account for flow resistance in natural channels due to bedforms. We found that the model predicted $\tau^*/\tau^*_{cr} > 1$ for four sites (1, 2, 14, and 15), three of which were the sites where active gravel transport was observed (Table S1).

As the Schneider et al. (2015) model best predicted where transport occurred on the fan during the August 2019 storm event, we used it to estimate sediment transport fluxes under both storm and bankfull conditions. For the storm event, sediment fluxes were effectively zero at all sites where we did not observe transport, and they were ~0.02–0.04 m^3/hr at the upper fan sites and ~0.01 m^3/hr at the lower site (Fig. 11B). Under bankfull conditions, the model predicts $0.5 < \tau^*/\tau^*_{cr} < 8.1$, where six sites have $\tau^*/\tau^*_{cr} \leq 1$ and negligible sediment fluxes. For the other 14 sites, bankfull sediment fluxes ranged from ~550 m^3/hr to 0.4 m^3/hr, with an average sediment flux of ~70 m^3/hr across the fan (Fig. 11B).

Intermittency

Based on our field observations and remote sensing mapping, we estimate that the upper fan contains ~0.019 km^3 of sediment, of which ~71% was deposited as debris flows (i.e., 0.14 km^3) and ~18% by fluvial processes (i.e., 0.003 km^3; the remaining 11% of the upper fan was mapped as soil). If we assume the lower fan is predominately fluvial in origin, then an

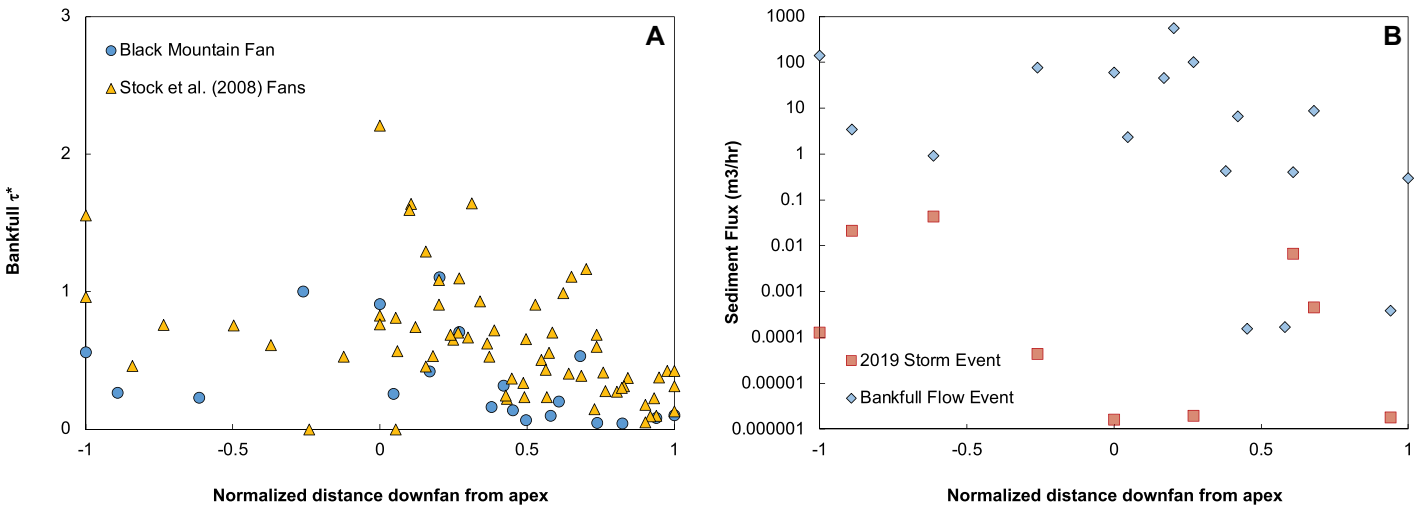

Figure 11. (A) The bankfull non-dimensional shear stress (bankfull Shields number, τ*) versus down-fan distance for both the Black Mountain fan and the fans investigated by Stock et al. (2008) show the decline in sediment transport capacity (due to hydraulic radius declining down-fan). (B) Sediment fluxes (in m^3 sediment/hr) using the Schneider et al. (2015) transport model going down-fan, both for the 2019 runoff event and under bankfull conditions.

additional 0.029 km^3 of sediment was deposited by river processes. In total, ~0.033 km^3 of the 0.049 km^3 fan, or ~67%, was likely fluvially deposited. Using Equation 12 and the Schneider et al. (2015) model for bankfull bedload flux, we estimate that the intermittency of sediment transporting flood events on the Black Mountain fan is ~0.2. It is less clear how often debris flow or mass flow events occur or what the average event size is (i.e., volume of sediment transported within a debris flow per flow event) without more detailed mapping and geochronological constraints, but our field observations suggest that smaller events may occur during summer storms, and larger events (like the 2016 landslide event) occur on an approximately decadal timescale (based on Google Earth time lapse imagery).

Water Budget

Using our estimates of bankfull water and sediment discharge, the average rock-to-water ratio (m^3 sediment/m^3 water) during fluvial flow events on the fan is 0.008 ± 0.02. We do not have field data on the range of rock-to-water ratio for debris and mudflows occurring within the Black Mountain catchment, but the typical range of rock-to-water ratios for granular debris flows and mudflows is 0.4–0.7 (Johnson, 1984; Whipple and Dunne, 1992; Morgan et al., 2014; Kaitna et al., 2016). In terms of the total water supply required to build the Black Mountain fan, this equates to a minimum of 4.1 km^3 (not accounting for water losses due to infiltration and evapotranspiration or flow events that do not transport sediment) or ~1 km (water volume/catchment area) of water.

DISCUSSION

Fan Morphology and Processes as a Function of Climate

Based on our surficial and sedimentological mapping, as well as models for the regional glaciation history (Lacelle et al., 2013), the Black Mountain fan has likely been forming under a periglacial climate over the last ~13,000 yr from a combination of mass flow and fluvial processes. Similar alluvial fan deposits have been found across a range of climates (e.g., Kochel and Johnson, 1984; Whipple and Dunne, 1992; Blair, 1999b; Crosta and Frattini, 2004) such that using the surface morphology or individual fluvial or debris flow deposits alone might make it difficult to discern environmental conditions at the time of deposition. Two exceptions, however, were for fluvial and debris flow-dominated periglacial fans in Svalbard (de Haas et al., 2015b). The first was in catchments where snow avalanches were prevalent and rapid beveling and leveling of inactive fan surfaces were observed. In these cases, coarse-grained debris flow levees were beveled down to stone stripes with reliefs of <10 cm. We did not observe evidence of this process on the Black Mountain fan, either in the field or from satellite imagery. Second, de Haas et al. (2015b) observed that most of the surfaces of the periglacial fans they studied in Svalbard were modified to some degree by solifluction, with areas of hummocky terrain and/or ice-wedge polygons, which were easily discerned in the field and could potentially be identified by remote sensing. Catto (1993) observed periglacial features on the Black Mountain fan in the early 1990s, but we found little evidence of these structures during the 2019 field season. The disappearance of evidence for periglacial modification of the Black Mountain fan over the last ~30 yr could be due to several reasons. First, the climate of the Aklavik Range has changed significantly enough to affect solifluction rates and the resulting surficial forms. Matsuoka (2001) found that surface velocities and sediment fluxes of soil are low when mean annual temperatures are <–6 °C but increase rapidly above –6 °C and reach a maximum with mean annual temperatures between –3 °C and –5 °C. Mean annual temperatures have increased by ~4 °C in the last ~60 yr at the Black Mountain fan site, and six of the last 10 years have had mean annual temperatures of between –3 °C and –6 °C, the range where hillslope transport rates have been shown to rapidly increase and hummocks are less commonly observed (Matsuoka, 2001). Second, the fan is currently more vegetated than it was previously (based on historical imagery and descriptions by Catto, 1993), which may obscure these features or affect solifluction processes (Matsuoka, 2001), though it is surprising that we do not see any evidence of the larger features (i.e., the spatulate projections of sediment mapped by Catto, 1993) in ArcticDEM topography.

Both Catto (1993) and de Haas et al. (2015b) suggest that debris flow size is likely to be restricted by active layer depths in periglacial environments, which could be a useful indicator of fan depositional setting. The presence and depth of the active layer is primarily controlled by surface mean annual temperature, the diurnal and annual surface temperature amplitude (i.e., temperature oscillations from low to high), snow cover, and the local geothermal gradient (Lachenbruch and Marshall, 1986). We estimated the annual-averaged modern active layer depth for the Black Mountain fan site to be ~1.5 m (Fig. 12) using a simple analytical diffusion model based on Anderson et al. (2013). This model predicts soil temperature at depth as a function of a sinusoidally varying surface temperature:

$$T(z,t) = \overline{T} + \Delta T e^{-z/z^*} \sin\left[\frac{2\pi t}{P} - \frac{z}{z^*}\right] \quad (13)$$

where $T(z,t)$ is the temperature at time, t, and depth, z, $\overline{T}$ is the mean temperature (−6 °C), ΔT is the temperature amplitude (15 °C), $z^* = \sqrt{\kappa P/\pi}$ is the depth scale, κ is the thermal diffusivity of the soil (1 mm^2/s), and P is the period of oscillation (1 yr). Snow cover was not accounted for due to the lack of snow cover thickness measurements at the site. This estimate for modern active layer depth suggests that individual debris flow deposits (or bed thicknesses) would be on the order of 1–2 m if they initiated due to the thawing of ground ice and failure along the permafrost table (which acts as an aquiclude), which notably falls within the typical range of observed bed thicknesses (i.e., 1–1.5 m). The thicker debris flow deposits we documented may be the result of successive active-layer failures, post-failure entrainment of sediment stored within the channel, rock fall contributions, warmer seasons, or flows that initiated from surface runoff and rapidly entrained talus/hillslope material.

There is a clear change in sediment transport processes between the steeper upper portion of the Black Mountain fan, which we interpret to be debris flow-dominated, to the shallower lower

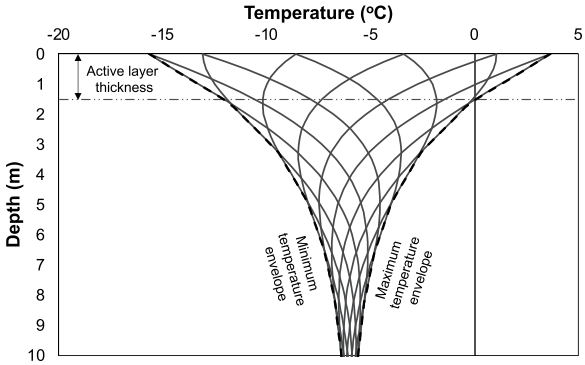

Figure 12. Modeled temperature profiles with depth at monthly intervals that span 1 yr are shown, where the mean annual temperature is assumed to be –6 °C and the temperature amplitude is ~15 °C. The estimated depth to the base of the active layer is indicated by the thin, dot-dashed black line (~1.5 m).

portion of the fan, which we interpret to be fluvially dominated. This process shift down-fan is also reflected in the fan's long profile (Fig. 3), where the upper fan has a mostly linear and long profile (typical debris flow fans) and the lower fan is concave-up in profile (associated with fluvial fans; Williams et al., 2011; de Haas et al., 2015b). However, without radiometric dating and drill core material, it is currently unclear if the lower and upper fan portions are coeval or if the unexposed sediments on the upper fan are of debris flow or fluvial origin.

One hypothesis is that accelerated warming has increased sediment supply, leading to aggradation and upper fan steepening. As the field site is located in a continuous permafrost region, physical weathering (i.e., frost cracking due to the presence of ice within bedrock) will dominate over chemical weathering in breaking down bedrock and generating sediment (Girard et al., 2013; Draebing and Krautblatter, 2019). Frost cracking tends to occur when water is present and rock temperatures are sustained below 0 °C, typically between −3 °C and −15 °C (Walder and Hallet, 1985; Rempel et al., 2016), and based on historical temperature data, the number of days in which the Black Mountain fan catchment is within the frost-cracking window has increased to about four additional weeks per year. The Black Mountain region also experiences bedrock landslide events that rapidly deliver large amounts of sediment downslope. The shale readily breaks down into fine-grained sediment that is both transported fluvially, as evidenced by an abundance of 3–4 mm shale grains within gravel bars, and by debris flows and mudflows, based on observed overbank deposits comprised predominantly of shale. Using Landsat imagery, we mapped five landslides along the Aklavik Range (not including the event within the Black Mountain fan catchment) that occurred in 2016, the warmest year on record over the past two decades. While these events could have been the result of tectonic activity, there were no locally recorded seismogenic events, and these landslides did not occur along a common fault trace or scarp, which suggests they were more likely related to the higher-than-normal temperatures. It is also possible that warming has led to more evapotranspiration due to increased vegetation, thereby reducing water availability within the actively thawing layer and leading to higher water-to-rock flow events.

An alternative hypothesis is that the upper and lower fan are coeval, and transport processes are closely tied to hydrologic conditions and/or sediment supply characteristics. For example, fluvial transport may dominate during spring snowmelt, as has been suggested by others for periglacial fan systems (Legget et al., 1966; Reiss et al., 2011; de Haas et al., 2015b), while debris flow events are more sporadic (initiating on steeper hillslopes and talus slopes as the active layer thaws) and take advantage of pre-existing fluvial channels as they transport down-fan. Debris flow formation also requires a wide coarse grain-size distribution and sufficient fine-grained material (i.e., clay and silt) to generate fluid pressures in excess of hydrostatic pressure and to increase the fluid yield strength (Pierson, 1981; Kaitna et al., 2016). As such, their occurrence may be more tied to the distribution of available grain sizes, as has been suggested for some temperate fans (e.g., Blair, 1999a, 2003). The Willow alluvial fan, located ~50 km north of the Black Mountain fan, shares a similar climate and tectonic history but features sedimentological data indicative primarily of fluvial deposits (Legget et al., 1966). Unlike the Black Mountain fan, the Willow fan does not significantly steepen in its upper portions. This may be due to the fact that the sediment available to the Willow fan is mostly clay to coarse sand with little coarse-grained material (Legget et al., 1966; Lane, 2005), thereby preventing granular debris flows.

Using Temperate Sediment Transport Models to Estimate Rates of Periglacial Fan Formation

Most bedload transport equations have not been applied to steep alluvial fans ($S > \sim 0.02$–0.03) due to limited observations of active sediment transport (e.g., Stock, 2013). In the few instances where sediment transport has been witnessed on fans, researchers have observed that: (1) reductions in local gradients due to loss of channel confinement led to the spread of flow, deposition of sediment into small dams, and subsequent flow bifurcation around the sediment dam (Eckis, 1928); (2) flow on fans tended to be supercritical (i.e., the Froude number, $Fr = \bar{u} / \sqrt{gh}$, is greater than 1) and could often transport particles with diameters approximately equal to the flow depth (Rahn, 1967; Beaumont and Oberlander, 1971; Stock, 2013); and (3) sediment concentrations varied during flow events, likely due to the occurrence of landsliding and debris flow events episodically contributing large pulses of sediment (Wasson, 1977; Stock, 2013). However, to the best of our knowledge, detailed measurements of channel hydraulic geometry and flow conditions during bedload transport have not been documented on steep periglacial fans, nor have sediment transport models, which were largely developed under temperate conditions for lower-gradient rivers, been tested.

The Stock et al. (2008) study is perhaps the most detailed regarding the measurement of down-fan changes in hydraulic geometry and particle size on temperate, arid alluvial fans. As such, we compare our findings from a periglacial fan to their study, which looked at four fans in the American southwest desert, to determine if and how fan morphology and sediment transport processes differ across these two climates. Stock et al. (2008) found that fan longitudinal profiles were concave-up, channel width-to-depth ratios ranged from 10 to 100 (similar to those of alluvial rivers; Knighton, 1998), there was a general down-fan decline in hydraulic radius, and there was a lack of gravel fining over the upper 60%–80% of the fan surfaces (but an increase in sand fraction; Figs. 4–5). In terms of sediment transport, Stock et al. (2008) showed that although sand fractions increased down-fan, which acts to reduce τ^*_c and increase transport capacity, this effect was not large enough to offset the decline in τ^* (Fig. 11), resulting in declining modeled sediment fluxes. We found that the Black Mountain fan also has (1) an overall concave-up profile (Fig. 3); (2) fan channels with width-to-depth ratios between 10 and 100 (though ~25% were below 10, which is characteristic of steep, mountainous channels (Palucis and Lamb, 2017); (3) a slight decrease in hydraulic radii down-fan; and (4) a lack of gravel fining but an increase in the fraction of sand down-fan (Figs. 4–5). As such, we confirm that bedload fluxes must be declining down-fan. Stock et al. (2008) proposed that the Mojave fans deposited large volumes of gravel down-fan via overbank deposition to match observed slope reductions. We observed overbank deposition along the Black Mountain fan, but it generally appeared to be associated with debris flow and mudflow events rather traction/sheet flow events. Stock et al. (2008) also tested a second hypothesis for controls on decreasing fan slope (i.e., the threshold hypothesis), where declining grain size, either due to shallowing flow or particle breakdown, leads to a reduction in slope. If this were the case, we would expect that slope would be an increasing function of the median grain size relative to the hydraulic radius, but we do not see this trend on either the Stock et al. (2008) fans or the Black Mountain fan (Fig. 13).

While there is a pronounced increase in the sand fraction of the channel bed as a function of down-fan distance, which should affect sediment fluxes by reducing the shear stress needed to initiate gravel transport, when we applied the Wilcock and Crowe (2003) model to the 2019 storm event it overpredicted where we observed bedload transport. This suggests that the presence of sand is being offset by other frictional losses within the channel, which are typically accounted for in bedload transport models by either reducing the acting bed shear stress or increasing τ^*_c. Both the Lamb et al. (2008) and

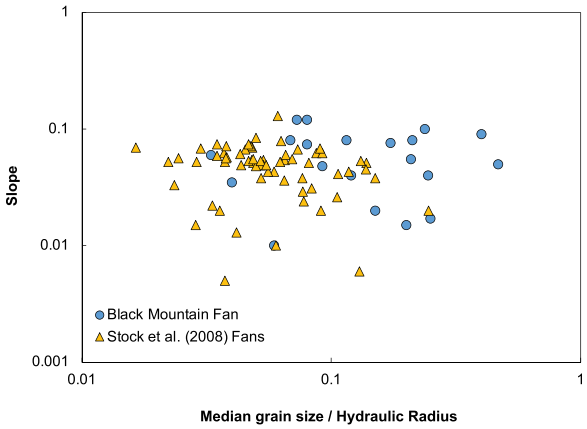

Figure 13. Plot of channel slope as a function of the median grain size (gravel fraction) relative to the hydraulic radius was used to test the Shield's threshold hypothesis for how channel slope declines down-fan. Similar to findings by Stock et al. (2008), we do not observe an increasing trend, which suggests that declining channel slope is not a function of declining grain size.

the Schneider et al. (2015) models we tested show a positive correlation between τ^*_c and slope (when τ^*_c is derived from total boundary shear stress), which has been suggested to be the result of increased drag on the walls of low width-to-depth channels (Vanoni and Brooks, 1957), steep channel bedforms (e.g., Montgomery and Buffington, 1997), grains emerging from steep and shallow flows (e.g., Yager et al., 2007), friction angle variations (e.g., Kirchner et al., 1990), increased relative roughness (D_{50}/h) (e.g., Prancevic and Lamb, 2015), and changes in flow structure and turbulence (Smith and McLean, 1977). The fact that the Schneider et al. (2015) model was more effective in predicting where sediment motion would occur could be because the data used to develop the Lamb et al. (2008) relation was a combination of flume and field data, with much of the field data plotted above the regression line for $S > 0.02$ (see their Fig. 1). The Schneider et al. (2015) model, however, used only field data (including steep stream environments), which thereby predicted a greater slope dependence on τ^*_c ($\tau^*_c \propto S^{0.5}$ versus $S^{0.25}$). This suggests that for natural channel slopes greater than ~0.02, such as the Black Mountain fan locality, macro-roughness elements in the channel or morphologic drag may be more important (Lamb et al., 2008; Schneider et al., 2015). As many of the Stock et al. (2008) fan channel slopes are also >0.02 (and contain bedforms), it is possible that the Schneider et al. (2015) model (or similar models that account for steep slopes and morphologic drag) would be appropriate for estimating sediment fluxes. As previously discussed, the Black Mountain catchment is prone to bedrock landsliding events, such as the 2016 landslide, which delivered a large amount of sediment to the fan three years prior to our field investigation. Pfeiffer et al. (2017) show that alluvial channels will often accommodate increases in sediment supply by reducing the bed surface median grain size (to increase flux) without changing channel geometry (i.e., local slope or channel width or depth). Future field studies will allow us to monitor if and how median grain sizes (and fluxes) change across the fan in response to this event.

Lastly, we note that the fluvial channel morphologies documented on the Black Mountain fan (i.e., cascade, step-pool, plane bed, and alternate bar) are found at channel bed slopes predicted by the model of Palucis and Lamb (2017) (Fig. 6). This model relates channel form to bed slope as a function of width-to-depth ratio, grain-size-to-width ratio, and Froude number. And while there is no fan equivalent to date of the bedform classifications for rivers (i.e., Montgomery and Buffington, 1997), our observations suggest that theory developed for fluvial systems may apply to steep alluvial fans, allowing for models to better account for macro-roughness and drag when estimating sediment fluxes.

Application to Martian Alluvial Fans

A key goal of this work was to assess the type, magnitude, and frequency of sediment transport processes and fluxes on an alluvial fan under a warming periglacial climate to determine the feasibility of martian fans having formed from limited meltwater (e.g., Kite et al., 2013). The type of flow events comprising these systems are particularly important because the rock-to-water volume ratios can vary by orders of magnitude between mass flow and fluvial processes. Terrestrial studies suggest that fan length and slope are two metrics that can be remotely sensed to provide insight into formational processes, with debris flow fans typically being shorter and steeper (>0.09–0.18) than their fluvially dominated counterparts (Williams et al., 2006; Stock et al., 2008; Stock, 2013). In their survey of 31 representative martian fans, Moore and Howard (2005) found that most fans had a slope of ~0.035, which is similar to the slopes measured on alluvial fans in Gale (0.009–0.035; Palucis et al., 2014), Saheki (0.035; Morgan et al., 2014), and Harris (0.04; Williams et al., 2011) craters. Many of these fans also have linear, ridge-like features that start at the fan's apexes, trend downslope with generally uniform widths, and contain bedform features such as scroll bars (e.g., Morgan et al., 2014; Palucis et al., 2014; Williams et al., 2011). This is consistent with channelized flow, and as such, these features have been interpreted as fluvial distributaries that carried coarse sediment down-fan and have since been inverted by aeolian erosion (Moore and Howard, 2005; Williams et al., 2009, 2011; Grant and Wilson, 2011). The overall low fan slopes and the presence of ridges have led many to the interpretation that most mid-latitude fan systems were fluvially dominated and would require significant volumes of water (e.g., Moore and Howard, 2005; Morgan et al., 2014; Palucis et al., 2014; Williams et al., 2011), with rock-to-water ratios of ~0.0001 based on typical terrestrial rivers (Syvitski et al., 2003).

Our geomorphic and sedimentological data suggest that while mass flow events are important in building the Black Mountain fan, the majority of the fan (~67%) still likely formed from fluvial processes (low rock-to-water ratios, ~0.008). This observation matches the low overall slope of the fan (~0.05) and the concavity of its profile. However, the remaining ~33% of the fan would have required rock-to-water ratios that are orders of magnitude higher, especially if debris flows were generated from the melting of interstitial ice and hillslope failures (versus high-intensity rainfall events as is often observed in temperate landscapes; Cannon et al., 2011; Staley et al., 2017; Berti et al., 2020). This emphasizes the importance of correctly interpreting the formative process, which is often difficult from a purely remote sensing approach. Had we assumed that low rock-to-water ratios were responsible for depositing the entire fan volume, we would have estimated that the Black Mountain fan required ~486 km^3 of water to form, which is vastly greater than our estimate of ~4 km^3.

Application of sediment transport models to martian fans requires knowledge of local channel slope, channel width and depth, and grain size, all of which easily can be collected in the field but are difficult to collect via orbital data. Currently, when transport models are applied to martian fans, the grain size and channel depth need to be assumed or are approximated from terrestrial fluvial data, typically from temperate river systems, resulting in flow estimates that can be off by orders of magnitude. Similarly, channel width is often used to estimate discharge, where $Q \sim bB^c$, and b and c are fit parameters from terrestrial systems that are scaled to account for differences in martian gravity (Irwin et al., 2005).

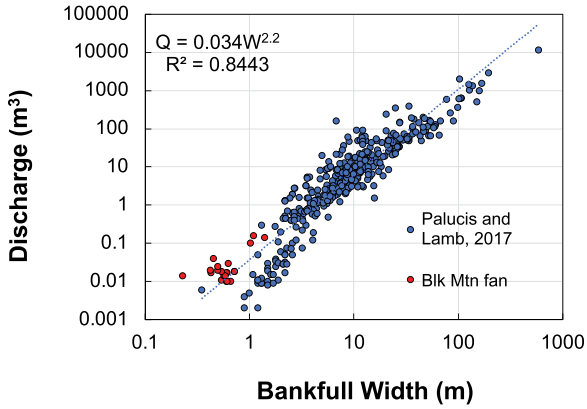

Figure 14. Bankfull discharge is shown as a function of bankfull channel width for steep, terrestrial alluvial streams (blue circles; Palucis and Lamb, 2017) and for the Black Mountain fan (red circles). The similar trend suggests that empirical relations between channel width and discharge for alluvial systems can be extended to steep alluvial fan systems.

Here, we have collected one of the most complete data sets on how channel slope, width-to-depth ratios, and grain size vary down a periglacial fan, and show that the trends are remarkably similar to those of more temperate to arid fan systems (Stock et al., 2008), which allows for a more robust estimate of these parameters when attempting to model water and sediment fluxes on martian fans. We also show in Figure 14 that discharge versus channel width relations for temperate steep streams (Palucis and Lamb, 2017) follow a similar relation to those observed on the Black Mountain fan. When adjusted for martian gravity using the relation by Burr et al. (2010):

$$\frac{B_M}{B_E} = \left(\frac{g_M}{g_E}\right)^{-0.233} \quad (14)$$

one can estimate average discharge on a martian alluvial channel fan from $Q = 0.03B^{2.2}$ by simply increasing the martian alluvial fan channel width by 1.25 (i.e., $Q_M = 0.03(1.25B_M)^{2.2}$). By relating flow discharge to upstream drainage area, we were able to estimate runoff rates downfan during a flow event (~0.01–0.1 mm/hr) and compare that to input rates (~1–2 mm/hr). This suggests that due to infiltration and evaporation, approximately an order of magnitude less water is available for transporting sediment and doing geomorphic work, which is an important consideration for Mars.

Early martian melt rates can be computed from climate models (e.g., Kite et al., 2013; Mansfield et al., 2018), but the water amount that is translated to surface runoff is not well constrained. Importantly, even under the range of runoff rates we estimated for the Black Mountain fan (~0.01 mm/hr to up ~10 mm/hr during bankfull conditions), we show that appreciable amounts of sediment can be transported (Fig. 11). Furthermore, the sediment transport analysis generated herein provides insight into how intermittent bankfull fluvial flow events occur on a periglacial fan. Within the Mars literature, intermittency factors are stated to range from 0.001 to 1, where the endmember case of $I_f = 1$ assumes constant bankfull flow (Hauber et al., 2009; Hoke et al., 2011; Orofino et al., 2018; Hayden et al., 2021); we show that on an alluvial fan system subject to cold and arid conditions, that value may be closer to ~0.2. If fans on Mars formed under similar settings, this would mean that warming conditions on Mars (perhaps from a combination of impact, volcanic, and seasonal forcing) would have needed to be sustained for an overall shorter period but likely for several weeks to months per year.

When considering whether the Black Mountain fan is an appropriate analog for martian fans, we acknowledge that the fan does have vegetation, which can affect subsurface water volumes (due to either water draw-down or evapotranspiration) and stabilize channel banks from erosion (Braudrick et al., 2009). Vegetation can also affect or hide surficial features indicative of periglacial processes, such that we cannot easily compare metrics like surface roughness between the Black Mountain fan and martian fans (though rapid climate shifts could have potentially muted periglacial features on both the Black Mountain fan as well as on fans on Mars; Matsuoka, 2001). We suggest, however, that the Black Mountain fan is an ideal martian analog in several other respects. First, it has average gradients similar to those of many martian fans (i.e., ~0.035–0.05), and its morphologic form is likely fluvially controlled. Second, the fan is predominately composed of fine-grained material, which has been inferred for martian alluvial fans due to the extent of inversion and presence of inverted channels, and it has an ephemeral distributary channel network. Third, the Black Mountain fan (as well as the other fans along the Aklavik Range) has a fan to catchment area scaling similar to that of martian fans (Fig. 1B), which suggests that similar erosional processes may have occurred on martian crater rims. Finally, and perhaps most importantly, the Black Mountain fan is an active snowmelt-fed fan that provides an ideal testing ground for continued work on how snowmelt-dominated systems affect sediment supply generation, the amount of liquid water available for sediment transport down-fan, and the frequency, duration, and magnitude of sediment transport events under changing climate.

CONCLUSIONS

Alluvial fans have the potential to record climate change through sediment and water delivery signals (via changing sediment fluxes or transport processes) on Earth and may represent one of the last widespread signs of fluvial activity on Mars' surface (e.g., Pepin et al., 2010; Armitage et al., 2011; D'Arcy et al., 2016). Understanding the climatic conditions during the formation of these features may provide key insights about habitability on Mars and climate change on Earth and Mars. It has been suggested that martian fans sourced water only from snowmelt and perhaps under periglacial conditions; however, numerous studies have used data and theory from terrestrial fans and rivers from warm, arid, rainfall-dominated climates to estimate flow discharges, runoff rates, and total water volumes to constrain martian fans. Here, we characterized the sedimentology and geomorphology of a periglacial alluvial fan in the Richardson Mountains, Northwest Territories, Canada, and presented novel data on how channel slope, channel width and depth, and grain size vary down-fan. The Black Mountain fan is predominately composed of fluvially deposited sediment (~67%) as opposed to being mostly debris flow deposits as previously suggested. Based on sediment transport observations from a mixed summer snowmelt and rainfall event within the Black Fan catchment (such observations are rare on alluvial fans), we were able to test several models for when bedload transport occurs. We found that the model of Schneider et al. (2015), which was developed using data from steep streams and accounts for macroroughness, was most applicable. The fan has an intermittency of ~0.2 regarding bankfull fluvial processes with episodic sediment flux inputs from mass flow processes. Based on our analysis, melt rates suggested for Mars are capable of entraining and transporting appreciable amounts of sediment by fluvial processes and under rock-to-water ratios that are about two orders of magnitude less than is often assumed based on averages from terrestrial rivers.

ACKNOWLEDGMENTS

This research was conducted at Dartmouth College, the University of Arkansas, Georgia Tech, and the Smithsonian Institute. Permission was granted to

do fieldwork on Gwich'in private lands through the Gwich'in Tribal Council (GTC19R001) and the Aurora Research Institute (16522). It was supported by a NASA Solar System Workings grant awarded to M.C. Palucis and J.V. Strauss (#80NSSC19K0539) and a National Science Foundation Office of Polar Programs grant awarded to M.C. Palucis, J.V. Strauss, and J. Marshall (NSF-OPP-ANS-2116471 and -21166571). We greatly appreciate the comments and suggestions provided by our reviewers. We thank Craig Nicholson at the Yukon Geological Survey, Galen Halverson (McGill University, Montréal, Québec, Canada), and Diane Wagner (NASA SUPPR program) for logistical support. A very special thanks is given to Sonny McDonald from the Gwich'in community of Akalvik, who helped collect field data and was our wildlife monitor during the 2019 field season. Data produced from this study is available at Figshare: https://figshare.com/s/83fc8aad3b228390e522.

REFERENCES CITED

Anderson, R.S., Anderson, S.P., and Tucker, G.E., 2013, Rock damage and regolith transport by frost: An example of climate modulation of the geomorphology of the critical zone: Earth Surface Processes and Landforms, v. 38, p. 299–316, https://doi.org/10.1002/esp.3330.

Armitage, J.J., Warner, N.H., Goddard, K., and Gupta, S., 2011, Timescales of alluvial fan development by precipitation on Mars: Geophysical Research Letters, v. 38, https://doi.org/10.1029/2011GL048907.

Bardou, E., and Delaloye, R., 2004, Effects of ground freezing and snow avalanche deposits on debris flows in Alpine environments: Natural Hazards and Earth System Sciences, v. 4, p. 519–530, https://doi.org/10.5194/nhess-4-519-2004.

Beaumont, P., and Oberlander, T., 1971, Observations on stream discharge and competence at Mosaic Canyon, Death Valley, California: Geological Society of America Bulletin, v. 82, p. 1695–1698, https://doi.org/10.1130/0016-7606(1971)82[1695:OOSDAC]2.0.CO;2.

Berti, M., Bernard, M., Gregoretti, C., and Simoni, A., 2020, Physical interpretation of rainfall thresholds for runoff-generated debris flows: Journal of Geophysical Research: Earth Surface, v. 125, https://doi.org/10.1029/2019JF005513.

Birch, S., Hayes, A., Howard, A., Moore, J., and Radebaugh, J., 2016, Alluvial fan morphology, distribution and formation on Titan: Icarus, v. 270, p. 238–247, https://doi.org/10.1016/j.icarus.2016.02.013.

Blair, T.C., 1999a, Cause of dominance by sheetflood vs. debris flow processes on two adjoining alluvial fans, Death Valley, California: Sedimentology, v. 46, p. 1015–1028, https://doi.org/10.1046/j.1365-3091.1999.00261.x.

Blair, T.C., 1999b, Sedimentology of the debris-flow-dominated Warm Spring Canyon alluvial fan, Death Valley, California: Sedimentology, v. 46, p. 941–965, https://doi.org/10.1046/j.1365-3091.1999.00260.x.

Blair, T.C., 2003, Features and origin of the giant Cucomungo Canyon alluvial fan, Eureka Valley, California, *in* Chan, M.A., and Archer, A.W., eds., Extreme Depositional Environments: Mega End Members in Geologic Time: Geological Society of America Special Paper 370, p. 105–126, https://doi.org/10.1130/0-8137-2370-1.105.

Blair, T.C., and McPherson, J.G., 2009, Processes and Forms of Alluvial Fans: Dordrecht, The Netherlands, Springer, p. 413–467, https://doi.org/10.1007/978-1-4020-5719-9_14.

Blissenbach, E., 1954, Geology of alluvial fans in semiarid regions: Geological Society of America Bulletin, v. 65, p. 175–190, https://doi.org/10.1130/0016-7606(1954)65[175:GOAFIS]2.0.CO;2.

Bonsal, B.R., and Kochtubajda, B., 2009, An assessment of present and future climate in the Mackenzie Delta and the near-shore Beaufort Sea region of Canada: International Journal of Climatology, v. 29, p. 1780–1795.

Braudrick, C.A., Dietrich, W.E., Leverich, G.T., and Sklar, L.S., 2009, Experimental evidence for the conditions necessary to sustain meandering in coarse-bedded rivers: Proceedings of the National Academy of Sciences of the United States of America, v. 106, p. 16,936–16,941, https://doi.org/10.1073/pnas.0909417106.

Bunte, K., and Abt, S.R., 2001, Sampling surface and subsurface particle-size distributions in wadable gravel- and cobble-bed streams for analyses in sediment transport, hydraulics, and streambed monitoring: U.S. Department of Agriculture, Forest Service, Rocky Mountain Research Station-General Technical Report 74, 428 p., https://doi.org/10.2737/RMRS-GTR-74.

Burr, D.M., Williams, R.M.E., Wendell, K.D., Chojnacki, M., and Emery, J.P., 2010, Inverted fluvial features in the Aeolis/Zephyria Plana region, Mars: Formation mechanism and initial paleodischarge estimates: Journal of Geophysical Research: Planets, v. 115, E07011, https://doi.org/10.1029/2009JE003496.

Cannon, S.H., Boldt, E.M., Laber, J.L., Kean, J.W., and Staley, D.M., 2011, Rainfall intensity—duration thresholds for postfire debris-flow emergency-response planning: Natural Hazards, v. 59, p. 209–236, https://doi.org/10.1007/s11069-011-9747-2.

Carr, M.H., 2012, The fluvial history of Mars: Philosophical Transactions of the Royal Society A: Mathematical, Physical and Engineering Sciences, v. 370, p. 2193–2215, https://doi.org/10.1098/rsta.2011.0500.

Carr, M.H., and Head, J.W., 2010, Geologic history of Mars: Earth and Planetary Science Letters, v. 294, p. 185–203, https://doi.org/10.1016/j.epsl.2009.06.042.

Cassidy, J.F., and Bent, A.L., 1993, Source parameters of the 29 May and 5 June, 1940 Richardson Mountains, Yukon Territory, earthquakes: Bulletin of the Seismological Society of America, v. 83, p. 636–659.

Cassidy, J.F., Rogers, G.C., and Ristau, J., 2005, Seismicity in the vicinity of the SNORCLE corridors of the northern Canadian Cordillera: Canadian Journal of Earth Sciences, v. 42, p. 1137–1148, https://doi.org/10.1139/e04-063.

Catto, N.R., 1993, Morphology and development of an alluvial fan in a permafrost region, Aklavik Range, Canada: Geografiska Annaler: Series A, Physical Geography, v. 75, p. 83–93, https://doi.org/10.1080/04353676.1993.11880387.

Cavalli, M., and Marchi, L., 2008, Characterisation of the surface morphology of an Alpine alluvial fan using airborne LiDAR: Natural Hazards and Earth System Sciences, v. 8, p. 323–333, https://doi.org/10.5194/nhess-8-323-2008.

Center, P.G., et al., 2018, Arctic DEM: Harvard Dataverse, v. 1.

Craddock, R.A., and Greeley, R., 2009, Minimum estimates of the amount and timing of gases released into the martian atmosphere from volcanic eruptions: Icarus, v. 204, p. 512–526, https://doi.org/10.1016/j.icarus.2009.07.026.

Crosta, G.B., and Frattini, P., 2004, Controls on modern alluvial fan processes in the Central Alps, Northern Italy: Earth Surface Processes and Landforms, v. 29, p. 267–293, https://doi.org/10.1002/esp.1009.

D'Arcy, M., Whittaker, A.C., and Roda-Boluda, D.C., 2016, Measuring alluvial fan sensitivity to past climate changes using a self-similarity approach to grain-size fining, Death Valley, California: Sedimentology: Journal of the International Association of Sedimentologists, v. 64, p. 388–424, https://doi.org/10.1111/sed.12308.

de Haas, T., Hauber, E., Conway, S., Van Steijn, H., Johnsson, A., and Kleinhans, M., 2015a, Earth-like aqueous debris-flow activity on Mars at high orbital obliquity in the last million years: Nature Communications, v. 6, 7543, https://doi.org/10.1038/ncomms8543.

de Haas, T., Kleinhans, M.G., Carbonneau, P.E., Rubensdotter, L., and Hauber, E., 2015b, Surface morphology of fans in the high-Arctic periglacial environment of Svalbard: Controls and processes: Earth-Science Reviews, v. 146, p. 163–182, https://doi.org/10.1016/j.earscirev.2015.04.004.

Dietrich, W.E., Palucis, M.C., Williams, R.M., Lewis, K.W., Rivera-Hernandez, F., and Sumner, D.Y., 2017, Fluvial gravels on Mars: Analysis and implications, *in* Tsusumi, D., and Laronne, J.B., eds., Gravel-Bed Rivers: Processes and Disasters: Hoboken, New Jersey, John Wiley & Sons, p. 755–783.

Dixon, J., 1986, Cretaceous to Pleistocene stratigraphy and paleogeography, northern Yukon and northwestern District of Mackenzie: Bulletin of Canadian Petroleum Geology, v. 34, p. 49–70.

Dixon, J., Dietrich, J., Snowdon, L.R., Morrell, G., and McNeil, D., 1992, Geology and petroleum potential of Upper Cretaceous and Tertiary strata, Beaufort-Mackenzie area, northwest Canada: American Association of Petroleum Geologists Bulletin, v. 76, p. 927–947.

Dixon, J., Dietrich, J., Lane, L., and McNeil, D., 2008, Geology of the Late Cretaceous to Cenozoic Beaufort-Mackenzie basin, Canada: Sedimentary Basins of the World, v. 5, p. 551–572, https://doi.org/10.1016/S1874-5997(08)00016-6.

Dixon, J., Lane, L., Dietrich, J., McNeil, D., and Chen, Z., 2019, Geological history of the Late Cretaceous to Cenozoic Beaufort-Mackenzie Basin, Arctic Canada, *in* The Sedimentary Basins of the United States and Canada: Amsterdam, Elsevier, p. 695–717, https://doi.org/10.1016/B978-0-444-63895-3.00017-6.

Draebing, D., and Krautblatter, M., 2019, The efficacy of frost weathering processes in Alpine rockwalls: Geophysical Research Letters, v. 46, p. 6516–6524.

Duk-Rodkin, A., and Hughes, O., 1991, Age relationships of Laurentide and montane glaciations, Mackenzie mountains, Northwest territories: Géographie Physique et Quaternaire, v. 45, p. 79–90, https://doi.org/10.7202/032847ar.

Duk-Rodkin, A., Barendregt, R.W., Froese, D.G., Weber, F., Enkin, R., Rod Smith, I., Zazula, G.D., Waters, P., and Klassen, R., 2004, Timing and extent of plio-pleistocene glaciations in north-western canada and east-central alaska, *in* Ehlers, J., and Gibbard, P.L. eds., Quaternary Glaciations-Extent and Chronology: Elsevier, Developments in Quaternary Sciences, v. 2, p. 313–345, https://doi.org/10.1016/S1571-0866(04)80206-9.

Eckis, R., 1928, Alluvial fans of the Cucamonga district, southern California: The Journal of Geology, v. 36, p. 224–247, https://doi.org/10.1086/623509.

Evans, J.E., 1991, Facies relationships, alluvial architecture, and paleohydrology of a Paleogene, humid-tropical alluvial-fan system: Chumstick Formation, Washington State, USA: Journal of Sedimentary Research, v. 61, p. 732–755.

Ferguson, R., 2007, Flow resistance equations for gravel- and boulder-bed streams: Water Resources Research, v. 43, W05427, https://doi.org/10.1029/2006WR005422.

Franke, D., Hornung, J., and Hinderer, M., 2015, A combined study of radar facies, lithofacies and three-dimensional architecture of an Alpine alluvial fan (Illgraben fan, Switzerland): Sedimentology, v. 62, p. 57–86, https://doi.org/10.1111/sed.12139.

French, H.M., 2017, The Periglacial Environment: Oxford, UK, John Wiley & Sons, https://doi.org/10.1002/9781119132820.

Garcia, M.H., 2008, Sediment transport and morphodynamics: Sedimentation engineering: Processes, measurements, modeling, and practice: American Society of Civil Engineers, ASCE Manuals and Reports on Engineering Practice No. 110, https://doi.org/10.1061/9780784408148.

Giles, P.T., 2010, Investigating the use of alluvial fan volume to represent fan size in morphometric studies: Geomorphology, v. 121, p. 317–328, https://doi.org/10.1016/j.geomorph.2010.05.001.

Girard, L., Gruber, S., Weber, S., and Beutel, J., 2013, Environmental controls of frost cracking revealed through in situ acoustic emission measurements in steep bedrock: Geophysical Research Letters, v. 40, p. 1748–1753, https://doi.org/10.1002/grl.50384.

Grant, J.A., and Wilson, S.A., 2011, Late alluvial fan formation in southern Margaritifer Terra, Mars: Geophysical Research Letters, v. 38, https://doi.org/10.1029/2011GL046844.

Grant, J.A., Wilson, S.A., Mangold, N., Calef, F., and Grotzinger, J.P., 2014, The timing of alluvial activity in Gale crater, Mars: Geophysical Research Letters, v. 41, p. 1142–1149, https://doi.org/10.1002/2013GL058909.

Harvey, A.M., 1997, The role of alluvial fans in arid zone fluvial systems, *in* Thomas, D.S.G., ed., Arid Zone Geomorphology: Process, Form and Change in Drylands (2nd edition): Chichester, UK, Wiley, p. 231–259.

Harvey, A.M., 1999, The occurrence and role of arid zone alluvial fans, *in* Thomas, D.S.G., ed., Arid Zone Geomorphology: New York, Halstead Press, p. 136–158.

Hauber, E., Gwinner, K., Kleinhans, M., Reiss, D., Di Achille, G., Ori, G.-G., Scholten, F., Marinangeli, L., Jaumann, R., and Neukum, G., 2009, Sedimentary deposits in Xanthe Terra: Implications for the ancient climate on Mars: Planetary and Space Science, v. 57, p. 944–957, https://doi.org/10.1016/j.pss.2008.06.009.

Hayden, A., Lamb, M., and McElroy, B., 2021, Constraining the timespan of fluvial activity from the intermittency of sediment transport on Earth and Mars: Geophysical Research Letters, v. 48, https://doi.org/10.1029/2021GL092598.

Hoke, M.R.T., Hynek, B.M., and Tucker, G.E., 2011, Formation timescales of large Martian valley networks: Earth and Planetary Science Letters, v. 312, p. 1–12, https://doi.org/10.1016/j.epsl.2011.09.053.

Holo, S.J., Kite, E.S., and Robbins, S.J., 2018, Obliquity history constrained by elliptic crater orientations: Earth and Planetary Science Letters, v. 496, p. 206–214, https://doi.org/10.1016/j.epsl.2018.05.046.

Holo, S.J., Kite, E.S., Wilson, S.A., and Morgan, A.M., 2021, The timing of alluvial fan formation on Mars: The Planetary Science Journal, v. 2, p. 210, https://doi.org/10.3847/PSJ/ac25ed.

Hutchinson, M.F., McKenney, D.W., Lawrence, K., Pedlar, J.H., Hopkinson, R.F., Milewska, E., and Papadopol, P., 2009, Development and testing of Canada-Wide interpolated spatial models of daily minimum–maximum temperature and precipitation for 1961–2003: Journal of Applied Meteorology and Climatology, v. 48, p. 725–741, https://doi.org/10.1175/2008JAMC1979.1.

Hyndman, R., Cassidy, J., Adams, J., Rogers, G., and Mazzotti, S., 2005, Earthquakes and seismic hazard in the Yukon-Beaufort-Mackenzie: Canadian Journal of Exploration Geophysics Recorder, v. 5, p. 32–66.

Ikeda, S., Parker, G., and Kimura, Y., 1988, Stable width and depth of straight gravel rivers with heterogeneous bed materials: Water Resources Research, v. 24, p. 713–722, https://doi.org/10.1029/WR024i005p00713.

Irwin, R.P., Craddock, R.A., and Howard, A.D., 2005, Interior channels in Martian valley networks: Discharge and runoff production: Geology, v. 33, p. 489–492, https://doi.org/10.1130/G21333.1.

Iverson, R.M., 1997, The physics of debris flows: Reviews of Geophysics, v. 35, p. 245–296, https://doi.org/10.1029/97RG00426.

Johnson, A.M., 1984, Debris Flows, *in* Brunsden, D., and Prior, D.B., eds., Slope Instability: New York, John Wiley, p. 257–361.

Kaitna, R., Palucis, M.C., Yohannes, B., Hill, K.M., and Dietrich, W.E., 2016, Effects of coarse grain size distribution and fine particle content on pore fluid pressure and shear behavior in experimental debris flows: Journal of Geophysical Research: Earth Surface, v. 121, https://doi.org/10.1002/2015JF003725.

Kirchner, J.W., Dietrich, W.E., Iseya, F., and Ikeda, H., 1990, The variability of critical shear stress, friction angle, and grain protrusion in water-worked sediments: Sedimentology, v. 37, p. 647–672, https://doi.org/10.1111/j.1365-3091.1990.tb00627.x.

Kite, E.S., Halevy, I., Kahre, M.A., Wolff, M.J., and Manga, M., 2013, Seasonal melting and the formation of sedimentary rocks on Mars, with predictions for the Gale crater mound: Icarus, v. 223, p. 181–210, https://doi.org/10.1016/j.icarus.2012.11.034.

Kite, E.S., Sneed, J., Mayer, D.P., and Wilson, S.A., 2017, Persistent or repeated surface habitability on Mars during the late Hesperian-Amazonian: Geophysical Research Letters, v. 44, p. 3991–3999, https://doi.org/10.1002/2017GL072660.

Knighton, A.D., 1998, Fluvial Forms and Processes: A New Perspective: London, Hodder Arnold Publications, 377 p.

Kochel, R.C., and Johnson, R.A., 1984, Geomorphology and sedimentology of humid-temperate alluvial fans, central Virginia, *in* Koster, E.H., and Steel, R.J., eds., Sedimentology of Gravels and Conglomerates: Canadian Society of Petroleum Geologists Memoir 10, p. 109–122.

Kraal, E.R., Asphaug, E., Moore, J.M., Howard, A., and Bredt, A., 2008, Catalogue of large alluvial fans in Martian impact craters: Icarus, v. 194, p. 101–110.

Lacelle, D., Lauriol, B., Zazula, G., Ghaleb, B., Utting, N., and Clark, I.D., 2013, Timing of advance and basal condition of the Laurentide Ice Sheet during the last glacial maximum in the Richardson Mountains, NWT: Quaternary Research, v. 80, p. 274–283, https://doi.org/10.1016/j.yqres.2013.06.001.

Lachenbruch, A.H., and Marshall, B.V., 1986, Changing climate: Geothermal evidence from permafrost in the Alaskan Arctic: Science, v. 234, p. 689–696, https://doi.org/10.1126/science.234.4777.689.

Lamb, M.P., Dietrich, W.E., and Venditti, J.G., 2008, Is the critical Shields stress for incipient sediment motion dependent on channel-bed slope?: Journal of Geophysical Research: Earth Surface, v. 113, F02008, https://doi.org/10.1029/2007JF000831.

Lane, L., 2005, Geology, Aklavik Range (107B/04), and part of adjacent Beaverhouse Creek (107B/05), District of Mackenzie, Northwest Territories: Geological Survey of Canada Open File 4827, https://doi.org/10.4095/216680.

Lane, L.S., and Issler, D.R., 2011, Overview of the Tertiary cooling-uplift history of Northernmost Yukon adjacent to the Beaufort Basin, based on apatite fission track studies: Abstract presented at CSPG/CSEG/CWLS Geoconvention 2011, 9–11 May, Calgary, Alberta, Canada, 3 p., https://geoconvention.com/2011-abstract-archive/.

Laskar, J., Correia, A.C.M., Gastineau, M., Joutel, F., Levrard, B., and Robutel, P., 2004, Long term evolution and chaotic diffusion of the insolation quantities of Mars: Icarus, v. 170, p. 343–364, https://doi.org/10.1016/j.icarus.2004.04.005.

Legget, R.F., Brown, R.E., and Johnston, G., 1966, Alluvial fan formation near Aklavik, Northwest Territories, Canada: Geological Society of America Bulletin, v. 77, p. 15–30, https://doi.org/10.1130/0016-7606(1966)77[15:AFFNAN]2.0.CO;2.

Leonard, L.J., Mazzotti, S., and Hyndman, R.D., 2008, Deformation rates estimated from earthquakes in the northern Cordillera of Canada and eastern Alaska: Journal of Geophysical Research: Solid Earth, v. 113.

Mangold, N., Kite, E.S., Kleinhans, M.G., Newsom, H., Ansan, V., Hauber, E., Kraal, E., Quantin, C., and Tanaka, K., 2012, The origin and timing of fluvial activity at Eberswalde crater, Mars: Icarus, v. 220, p. 530–551, https://doi.org/10.1016/j.icarus.2012.05.026.

Mansfield, M., Kite, E.S., and Mischna, M.A., 2018, Effect of Mars atmospheric loss on snow melt potential in a 3.5 Gyr Mars climate evolution model: Journal of Geophysical Research: Planets, v. 123, p. 794–806, https://doi.org/10.1002/2017JE005422.

Matsuoka, N., 2001, Solifluction rates, processes and landforms: A global review: Earth-Science Reviews, v. 55, p. 107–134, https://doi.org/10.1016/S0012-8252(01)00057-5.

McKay, R., Enkelmann, E., Hadlari, T., Matthews, W., and Mouthereau, F., 2021, Cenozoic exhumation history of the eastern margin of the northern Canadian Cordillera: Tectonics, v. 40, https://doi.org/10.1029/2020TC006582.

Montgomery, D.R., and Buffington, J.M., 1997, Channel-reach morphology in mountain drainage basins: Geological Society of America Bulletin, v. 109, p. 596–611, https://doi.org/10.1130/0016-7606(1997)109<0596:CRMIMD>2.3.CO;2.

Moore, J.M., and Howard, A.D., 2005, Large alluvial fans on Mars: Journal of Geophysical Research: Planets, v. 110, https://doi.org/10.1029/2004JE002352.

Morgan, A.M., and Wilson, S.A., 2019, Utilizing a global database to explore morphologic trends of martian alluvial fans, *in* Lunar and Planetary Science Conference 50, The Woodlands, Texas, LPI Contribution No. 3256.

Morgan, A.M., Howard, A.D., Hobley, D.E.J., Moore, J.M., Dietrich, W.E., Williams, R.M.E., Burr, D.M., Grant, J.A., Wilson, S.A., and Matsubara, Y., 2014, Sedimentology and climatic environment of alluvial fans in the Martian Saheki crater and a comparison with terrestrial fans in the Atacama Desert: Icarus, v. 229, p. 131–156, https://doi.org/10.1016/j.icarus.2013.11.007.

Morgan, A., Wilson, S., Howard, A., Craddock, R., and Grant, J., 2018, Global distribution of alluvial fans and deltas on Mars, *in* Lunar and Planetary Science Conference 49, LPI Contribution No. 2083.

Noh, M.-J., and Howat, I.M., 2015, Automated stereo-photogrammetric DEM generation at high latitudes: Surface extraction with TIN-based Search-Space Minimization (SETSM) validation and demonstration over glaciated regions: GIScience & Remote Sensing, v. 52, p. 198–217, https://doi.org/10.1080/15481603.2015.1008621.

Okulitch, A., and Irwin, D., 2014, Geological compilation of the Western Mainland and Southern Arctic Islands regions, Northwest Territories: NWT Open File 2014-01.

Ori, G.G., 1982, Braided to meandering channel patterns in humid-region alluvial fan deposits, River Reno, Po Plain (northern Italy): Sedimentary Geology, v. 31, p. 231–248, https://doi.org/10.1016/0037-0738(82)90059-8.

Orofino, V., Alemanno, G., Di Achille, G., and Mancarella, F., 2018, Estimate of the water flow duration in large Martian fluvial systems: Planetary and Space Science, v. 163, p. 83–96, https://doi.org/10.1016/j.pss.2018.06.001.

O'Sullivan, P.B., and Lane, L.S., 1997, Early Tertiary thermotectonic history of the northern Yukon and adjacent Northwest Territories, Arctic Canada: Canadian Journal of Earth Sciences, v. 34, p. 1366–1378, https://doi.org/10.1139/e17-109.

Palucis, M., and Lamb, M., 2017, What controls channel form in steep mountain streams?: Geophysical Research Letters, v. 44, p. 7245–7255, https://doi.org/10.1002/2017GL074198.

Palucis, M.C., Dietrich, W.E., Hayes, A.G., Williams, R.M.E., Gupta, S., Mangold, N., Newsom, H., Hardgrove, C., Calef, F., and Sumner, D.Y., 2014, The origin and evolution of the Peace Vallis fan system that drains to the Curiosity landing area, Gale crater, Mars: Journal of Geophysical Research: Planets, v. 119, https://doi.org/10.1002/2013JE004583.

Paola, C., Heller, P.L., and Angevine, C.L., 1992, The large-scale dynamics of grain-size variation in alluvial basins, 1: Theory: Basin Research, v. 4, p. 73–90, https://doi.org/10.1111/j.1365-2117.1992.tb00145.x.

Parker, G., 1978, Self-formed straight rivers with equilibrium banks and mobile bed. Part 2. The gravel river: Journal of Fluid Mechanics, v. 89, p. 127–146, https://doi.org/10.1017/S0022112078002505.

Parker, G., 2008, 3—Transport of gravel and sediment mixtures, *in* García, M.H., ed., Sedimentation Engineering—Processes, Measurements, Modeling, and Practice: Reston, Virginia, American Society of Civil Engineers, p. 165–251, https://doi.org/10.1061/9780784408148.ch03.

Parker, G., Wilcock, P.R., Paola, C., Dietrich, W.E., and Pitlick, J., 2007, Physical basis for quasi-universal relations describing bankfull hydraulic geometry of single-thread gravel bed rivers: Journal of Geophysical Research: Earth Surface, v. 112, F04005, https://doi.org/10.1029/2006JF000549.

Pepin, E., Carretier, S., and Herail, G., 2010, Erosion dynamics modelling in a coupled catchment-fan system with constant external forcing: Geomorphology, v. 122, p. 78–90, https://doi.org/10.1016/j.geomorph.2010.04.029.

Pfeiffer, A.M., Finnegan, N.J., and Willenbring, J.K., 2017, Sediment supply controls equilibrium channel geometry in gravel rivers: Proceedings of the National Academy of Sciences of the United States of America, v. 114, p. 3346–3351, https://doi.org/10.1073/pnas.1612907114.

Pierson, T.C., 1981, Dominant particle support mechanisms in debris flows at Mt Thomas, New Zealand, and implications for flow mobility: Sedimentology, v. 28, p. 49–60, https://doi.org/10.1111/j.1365-3091.1981.tb01662.x.

Prancevic, J.P., and Lamb, M.P., 2015, Particle friction angles in steep mountain channels: Journal of Geophysical Research: Earth Surface, v. 120, p. 242–259, https://doi.org/10.1002/2014JF003286.

Radebaugh, J., et al., 2013, Alluvial fans on Titan reveal materials, processes and regional conditions, *in* 44th Lunar and Planetary Science Conference, Lunar Planetary

Institute, LPI-Contribution, https://www.lpi.usra.edu/meetings/lpsc2013/pdf/2641.pdf.

Rahn, P.H., 1967, Sheetfloods, streamfloods, and the formation of pediments: Annals of the Association of American Geographers, v. 57, p. 593–604, https://doi.org/10.1111/j.1467-8306.1967.tb00624.x.

Reiss, D., et al., 2011, Terrestrial gullies and debris-flow tracks on Svalbard as planetary analogs for Mars, *in* Garry, W.B., and Bleacher, J.E., Analogs for Planetary Exploration: Geological Society of America Special Paper 483, p. 165–175, https://doi.org/10.1130/2011.2483(11).

Rempel, A.W., Marshall, J.A., and Roering, J.J., 2016, Modeling relative frost weathering rates at geomorphic scales: Earth and Planetary Science Letters, v. 453, p. 87–95, https://doi.org/10.1016/j.epsl.2016.08.019.

Schneider, J.M., Rickenmann, D., Turowski, J.M., Bunte, K., and Kirchner, J.W., 2015, Applicability of bed load transport models for mixed-size sediments in steep streams considering macro-roughness: Water Resources Research, v. 51, p. 5260–5283, https://doi.org/10.1002/2014WR016417.

Segura, T.L., Toon, O.B., and Colaprete, A., 2008, Modeling the environmental effects of moderate-sized impacts on Mars: Journal of Geophysical Research: Planets, v. 113, E11007, https://doi.org/10.1029/2008JE003147.

Seizilles, G., Devauchelle, O., Lajeunesse, E., and Métivier, F., 2013, Width of laminar laboratory rivers: Physical Review E, v. 87, https://doi.org/10.1103/PhysRevE.87.052204.

Selby, M.J., 1993, Hillslope Materials and Processes: Oxford, UK, Oxford University Press, 451 p.

Shields, A., 1936, Application of Similarity Principles and Turbulence Research to Bed-Load Movement: Pasadena, California, California Institute of Technology, https://resolver.caltech.edu/CaltechKHR:HydroLabpub167.

Smith, J.D., and McLean, S., 1977, Spatially averaged flow over a wavy surface: Journal of Geophysical Research, v. 82, p. 1735–1746.

Staley, D.M., Negri, J.A., Kean, J.W., Laber, J.L., Tillery, A.C., and Youberg, A.M., 2017, Prediction of spatially explicit rainfall intensity—duration thresholds for post-fire debris-flow generation in the western United States: Geomorphology, v. 278, p. 149–162, https://doi.org/10.1016/j.geomorph.2016.10.019.

Stock, J., 2013, 9.23 Waters Divided: A history of alluvial fan research and a view of its future, *in* Shroder, J.F., ed., Treatise on Geomorphology, Volume 9: Cambridge, Massachusetts, Academic Press, p. 413–458.

Stock, J.D., Schmidt, K.M., and Miller, D.M., 2008, Controls on alluvial fan long-profiles: Geological Society of America Bulletin, v. 120, p. 619–640, https://doi.org/10.1130/B26208.1.

Syvitski, J.P., Peckham, S.D., Hilberman, R., and Mulder, T., 2003, Predicting the terrestrial flux of sediment to the global ocean: A planetary perspective: Sedimentary Geology, v. 162, p. 5–24, https://doi.org/10.1016/S0037-0738(03)00232-X.

Tarboton, D.G., 1997, A new method for the determination of flow directions and upslope areas in grid digital elevation models: Water Resources Research, v. 33, p. 309–319, https://doi.org/10.1029/96WR03137.

Tomczyk, A.M., and Ewertowski, M.W., 2017, Surface morphological types and spatial distribution of fan-shaped landforms in the periglacial high-Arctic environment of central Spitsbergen, Svalbard: Journal of Maps, v. 13, p. 239–251, https://doi.org/10.1080/17445647.2017.1294543.

Tomczyk, A.M., Ewertowski, M.W., Stawska, M., and Rachlewicz, G., 2019, Detailed alluvial fan geomorphology in a high-Arctic periglacial environment, Svalbard: Application of unmanned aerial vehicle (UAV) surveys: Journal of Maps, v. 15, p. 460–473, https://doi.org/10.1080/17445647.2019.1611498.

Toon, O.B., Segura, T., and Zahnle, K., 2010, The formation of Martian river valleys by impacts: Annual Review of Earth and Planetary Sciences, v. 38, p. 303–322, https://doi.org/10.1146/annurev-earth-040809-152354.

Turbet, M., Forget, F., Head, J.W., and Wordsworth, R., 2017, 3D modelling of the climatic impact of outflow channel formation events on early Mars: Icarus, v. 288, p. 10–36, https://doi.org/10.1016/j.icarus.2017.01.024.

Vanoni, V.A., and Brooks, N.H., 1957, Laboratory studies of the roughness and suspended load of alluvial streams: California Institute of Technology Report E-68, 130 p., https://resolver.caltech.edu/CaltechKHR:SedLabRpt-E-68.

Walder, J., and Hallet, B., 1985, A theoretical model of the fracture of rock during freezing: Geological Society of America Bulletin, v. 96, p. 336–346, https://doi.org/10.1130/0016-7606(1985)96<336:ATMOTF>2.0.CO;2.

Wasson, R., 1977, Last-glacial alluvial fan sedimentation in the Lower Derwent Valley, Tasmania: Sedimentology, v. 24, p. 781–799, https://doi.org/10.1111/j.1365-3091.1977.tb01915.x.

Weiss, D.K., and Head, J.W., 2017, Evidence for stabilization of the ice-cemented cryosphere in earlier Martian history: Implications for the current abundance of groundwater at depth on Mars: Icarus, v. 288, p. 120–147, https://doi.org/10.1016/j.icarus.2017.01.018.

Whipple, K.X., and Dunne, T., 1992, The influence of debris-flow rheology on fan morphology, Owens Valley, California: Geological Society of America Bulletin, v. 104, p. 887–900, https://doi.org/10.1130/0016-7606(1992)104<0887:TIODFR>2.3.CO;2.

Wilcock, P.R., and Crowe, J.C., 2003, Surface-based transport model for mixed-size sediment: Journal of Hydraulic Engineering, v. 129, p. 120–128, https://doi.org/10.1061/(ASCE)0733-9429(2003)129:2(120).

Williams, R.M., Zimbelman, J.R., and Johnston, A.K., 2006, Aspects of alluvial fan shape indicative of formation process: A case study in southwestern California with application to Mojave crater fans on Mars: Geophysical Research Letters, v. 33, https://doi.org/10.1029/2005GL025618.

Williams, R.M., Irwin, R.P., and Zimbelman, J.R., 2009, Evaluation of paleohydrologic models for terrestrial inverted channels: Implications for application to Martian sinuous ridges: Geomorphology, v. 107, p. 300–315, https://doi.org/10.1016/j.geomorph.2008.12.015.

Williams, R.M., Rogers, A.D., Chojnacki, M., Boyce, J., Seelos, K.D., Hardgrove, C., and Chuang, F., 2011, Evidence for episodic alluvial fan formation in far western Terra Tyrrhena, Mars: Icarus, v. 211, p. 222–237, https://doi.org/10.1016/j.icarus.2010.10.001.

Williams, R.M. et al., 2013, Martian fluvial conglomerates at Gale crater: Science, v. 340, p. 1068–1072.

Wilson, S.A., Morgan, A.M., Howard, A.D., and Grant, J.A., 2021, The global distribution of craters with alluvial fans and deltas on Mars: Geophysical Research Letters, v. 48, https://doi.org/10.1029/2020GL091653.

Wordsworth, R.D., 2016, The climate of early Mars: Annual Review of Earth and Planetary Sciences, v. 44, p. 381–408, https://doi.org/10.1146/annurev-earth-060115-012355.

Yager, E.M., Kirchner, J.W., and Dietrich, W.E., 2007, Calculating bed load transport in steep boulder bed channels: Water Resources Research, v. 43, W07418, https://doi.org/10.1029/2006WR005432.

Science Editor: Mihai Ducea
Associate Editor: Emmanuel Gabet

Manuscript Received 17 January 2022
Revised Manuscript Received 25 April 2022
Manuscript Accepted 12 May 2022

Printed in the USA